Oceanic Turbulence and Stochastic Models from Subsurface Lagrangian Data for the Northwest Atlantic Ocean

MILENA VENEZIANI

Division of Meteorology and Physical Oceanography, Rosenstiel School of Marine and Atmospheric Science, University of Miami, Miami, Florida

ANNALISA GRIFFA

Division of Meteorology and Physical Oceanography, Rosenstiel School of Marine and Atmospheric Science, University of Miami, Miami, Florida, and IOF/CNR, La Spezia, Italy

ANDY M. REYNOLDS

Silsoe Research Institute, Silsoe, Bedford, United Kingdom

ARTHUR J. MARIANO

Division of Meteorology and Physical Oceanography, Rosenstiel School of Marine and Atmospheric Science, University of Miami, Miami, Florida

(Manuscript received 9 May 2003, in final form 13 January 2004)

ABSTRACT

The historical dataset provided by 700-m acoustically tracked floats is analyzed in different regions of the northwestern Atlantic Ocean. The goal is to characterize the main properties of the mesoscale turbulence and to explore Lagrangian stochastic models capable of describing them. The data analysis is carried out mostly in terms of Lagrangian velocity autocovariance and cross-covariance functions. In the Gulf Stream recirculation and extension regions, the autocovariances and cross covariances exhibit significant oscillatory patterns on time scales comparable to the Lagrangian decorrelation time scale. They are indicative of sub- and superdiffusive behaviors in the mean spreading of water particles. The main result of the paper is that the properties of Lagrangian data can be considered as a superposition of two different regimes associated with looping and nonlooping trajectories and that both regimes can be parameterized using a simple first-order Lagrangian stochastic model with spin parameter Ω. The spin couples the zonal and meridional velocity components, reproducing the effects of rotating coherent structures such as vortices and mesoscale eddies. It is considered as a random parameter whose probability distribution is approximately bimodal, reflecting the distribution of loopers (finite Ω) and nonloopers (zero Ω). This simple model is found to be very effective in reproducing the statistical properties of the data.

1. Introduction

Lagrangian data provide direct information on ocean currents in terms of velocity and transport. Extensive historical datasets are available today, both at and below the ocean surface [useful information and lists of references can be found online at the following Web sites: Drifting Buoy Data Assembly Center (Atlantic Oceanographic and Meteorological Laboratory, Miami, Florida), http://www.aom1.noaa.gov/phod/dac/dac.html; Subsurface Float Data Center (Woods Hole, Massachusetts), http://wfdac.whoi.edu], and their statistical analyses have contributed significantly to improving our knowledge of the ocean circulation (e.g., Patterson 1985; Davis 1991; Owens 1991; Swenson and Niiler 1996; Bauer et al. 1998; Lavender et al. 2000; Poulain 2001; Fratantoni 2001; Bower et al. 2002). Lagrangian instruments are particularly suitable for transport and mixing studies because they move approximately with the ocean currents on (sub) mesoscale time scales (Davis 1991; Riser 1982). In a number of previous investigations (e.g., Freeland et al. 1975; Riser and Rossby 1983; Krauss and Boning 1987; Zhang et al. 2001; Bauer et al. 2002), mostly focused on the ocean surface, Lagrangian data have been used to characterize transport properties related to mesoscale turbulence and to test possible parameterization methods. Turbulence param-

Corresponding author address: Milena Veneziani, RSMAS/MPO 4600 Rickenbacker Causeway, Miami, FL 33149.
E-mail: cveneziani@rsmas.miami.edu

eterizations are crucial for climate applications of ocean general circulation models (OGCMs), since the eddy field is usually not resolved and the results rely heavily upon the correct representation of the eddy effects on the simulated large-scale circulation.

The simplest possible parameterization of turbulent transport is through the commonly used ''eddy diffusivity,'' which neglects correlations between successive velocity fluctuations. This approach cannot be used to model transport processes on time scales shorter than the integral Lagrangian time scale, and over which velocity fluctuations remain significantly correlated. Furthermore, the eddy-diffusivity approximation is not readily extended to include the influence of non-Gaussian velocity statistics and particle inertia (e.g., Tennekes and Lumley 1972). An alternative class of parameterization methods that are easily generalizable and have a wide applicability is based on Markovian stochastic models describing the motion of single particles in turbulent flows (e.g., Risken 1989). These models have been widely used in applications in physics of the atmosphere (e.g., Thomson 1987) and in oceanography (e.g., Griffa 1996), and within this context they are often referred to as Lagrangian stochastic (LS) models (Sawford 1991). A hierarchy of LS models can be derived by increasing the order of the joint Markovian variables, providing a means of reproducing increasingly more complex statistical properties.

Previous results on the analysis of surface Lagrangian data (e.g., Krauss and Boning 1987; Poulain and Niiler 1989; Figueroa and Olson 1989; Falco et al. 2000) suggest that, away from strong shear currents and from the equatorial regions, turbulent processes can be modeled by using a simple, one-dimensional, first-order LS model. This implies that the two velocity components of the fluctuation field are independent (one dimensionality), and that the position $\mathbf{x}$ and the velocity $\mathbf{u}'$ evolve jointly as a Markovian process (first-order property). Lagrangian velocity autocovariance functions are exponential, with an *e*-folding scale equal to the decorrelation time scale T_L, while diffusion processes are ballistic at short times (i.e., the mean particle dispersion[1] $\langle x^2 \rangle$ is proportional to t^2, for $t \ll T_L$) and diffusive at longer times ($\langle x^2 \rangle \propto t$, for $t \gg T_L$). These models describe ''simple'' situations of well-developed turbulence in the absence of coherent structures.

Such a description does not apply when the eddy dynamics is characterized by the presence of coherent structures. This is the case, for instance, in the equatorial Pacific (Bauer et al. 1998, 2002), where the flow is dominated by wave activity. Lagrangian data in this area give rise to strongly oscillating autocovariance functions, and to an intermediate time regime of anomalous diffusion, primarily subdiffusive, due to the trapping of particles in the wave field. Coherent structures are also expected to play an important role at midlatitudes where instabilities of strong shear currents (e.g., the western boundary currents extensions) lead to the formation of intense vortices such as Gulf Stream rings.

Suitable parameterizations of turbulent processes in the presence of coherent structures are still under debate. Berloff and McWilliams (2002), on the basis of numerical trajectories simulated in a double-gyre model, have suggested the use of one-dimensional, higher-order LS models. A possible application of this kind of model to the equatorial Pacific data is discussed in Bauer et al. (2002). Alternatively, Reynolds (2002a) has considered the use of two-dimensional, first-order LS models. In this case, the coherent structure effects are modeled through the correlation between the eddy velocity components, which determines a rotational motion of the trajectories. Other authors have suggested that quasi-geostrophic or two-dimensional turbulence might be considered as a suitable paradigm for the interpretation of oceanic turbulence (Elhmaidi et al. 1993; Provenzale 1999; Reynolds 2002b), so that appropriate parameterization models should take into account non-Gaussianities and the existence of at least two different regimes, one associated with the strong coherent vortices and the other related to the more quiescent background (Pasquero et al. 2001). Non-Gaussianities have indeed been seen in the analysis of subsurface float data in the North Atlantic (Bracco et al. 2000), as well as in numerical trajectories simulated by a high-resolution model (Bracco et al. 2003). Furthermore, Richardson (1993) has identified two distinct classes of trajectories in the subsurface float data. He has classified the floats as ''loopers'' and ''nonloopers,'' recognizing that many trajectories experienced marked looping behaviors due to the trapping effects of strong vortices.

A definitive answer to which model and which physical interpretation of mesoscale turbulence is the most appropriate cannot be given at this stage because not enough evidence from the data is available. The need for data analyses that specifically test the various hypotheses provides motivation for the present work.

In this paper, the question of how to characterize and parameterize oceanic turbulence in the presence of coherent structures is addressed by considering the historical dataset of subsurface floats at 700-m depth in the northwest Atlantic. The goal is twofold. On the one side, we aim at better understanding oceanic turbulence, and, by characterizing it in terms of stochastic models, we verify hypotheses on its degree of complexity and on the nature of the coherent structures. For simplicity, we focus on specific geographical subregions that are ''quasi homogeneous'' in terms of dynamics and statistics, so that the applications can be considered in good approximation as ''local.'' On the other side, the work will also provide indications on which type of transport model is most suitable for coarse-grain GCMs to simulate subgrid-scale transport by unresolved (or partially resolved) mesoscale eddies. Our results can be considered

[1] The angle brackets used here, and elsewhere in this paper, denote some kind of ensemble average.

as a first step in this direction. The actual use of LS models in OGCMs will involve ''global'' applications, where the spatial inhomogeneities will have to be included (Berloff and McWilliams 2002).

We concentrate on the regions of the Gulf Stream extension and recirculation because they are characterized by the presence of strong vortices and rings as clearly illustrated by the large number of looping trajectories (Richardson 1993) and as seen in satellite images (Brown et al. 1986). We focus on the statistical properties of the eddy turbulent field $\mathbf{u}'$, estimated as a residual from the mean flow $\mathbf{U}$ in each of the geographical subregions mentioned above. After a preliminary analysis to verify that the properties of the eddy field are independent from the averaging process of the mean flow estimation, the $\mathbf{u}'$ statistics are computed in terms of autocovariance and cross-covariance functions. The analyses are performed over the whole trajectory ensemble, and separately over the looper and nonlooper subsets. They are then used to identify suitable Lagrangian stochastic models capable of describing the statistics of observed covariability.

The paper is organized as follows. The first part provides a background overview on LS models (section 2), while the second part is devoted to the Lagrangian data analysis. In section 3, information on the data and on the methodology used to compute the mean flow is provided. The results from the statistical analysis of the eddy field are shown in section 4, together with the tests on Lagrangian stochastic model applicability. In section 5, a discussion on the properties of the loopers and nonloopers populations is presented. A summary and a brief discussion on open questions and future developments are provided in section 6.

2. Lagrangian stochastic models

Material transport in inhomogeneous, nonstationary turbulence, typical of oceanic gyres, is most readily predicted from the trajectories of particles simulated by Lagrangian stochastic models (e.g., Griffa 1996). The simplest such model is the random walk or zeroth-order LS model in which successive increments in the position of a particle are taken to be uncorrelated and the particle position is modeled as a Markovian process.

A time scale representative of the ''energy containing'' scales of motions is introduced at first order. In these models, particle positions and velocities evolve jointly as a continuous Markovian process. This is justifiable only when the Lagrangian acceleration autocorrelation function approaches a δ function at the origin, corresponding to an uncorrelated component in the acceleration and hence to a Markov process (Sawford 1991). At second order, particle positions, velocities, and accelerations evolve jointly as a Markovian process (Sawford 1991; Berloff and McWilliams 2002). Mathematically, at least, this hierarchy of models can be extended to higher orders (Berloff and McWilliams 2002; Reynolds 2003a).

Notice that there is a correspondence between LS models, which are stochastic differential equations describing particle motion in a turbulent flow, and Fokker–Planck (or Kolmogorov) equations, which are partial differential equations describing the particle probability density function (pdf) in the appropriate space (e.g., Risken 1989). For zeroth-order models, the appropriate space is simply the physical space ($\mathbf{x}$) and the Fokker–Planck equation corresponds to the commonly used advection–diffusion equation. For first-order models, the ($\mathbf{x}$, $\mathbf{u}'$) space has to be considered, while for second-order models, the acceleration is also included ($\mathbf{x}$, $\mathbf{u}'$, $\mathbf{A}$). In practical applications like the present one, the LS model formulation appears more natural than the Fokker–Planck equation approach because, aside from being easier to implement, it provides a direct way to test the model and compare it with Lagrangian observations in terms of particle trajectories and autocorrelation functions.

First-order models are generally prescribed by

$$du_i' = a_i(\mathbf{u}', \mathbf{x}, t)dt + b_{ij}(\mathbf{u}', \mathbf{x}, t)d\xi_j, \qquad (1)$$

where $\mathbf{u}'(t)$ is the Lagrangian turbulent velocity of a particle (hereinafter the primes will be dropped for simplicity of notation), $\mathbf{x}(t)$ is the particle position along a trajectory, t is time, and $d\xi$ is an incremental Weiner process with independent components, having 0 mean and variance dt.

One of the constraints that determine the precise form of the model is the well-mixed condition (Thomson 1987). The well-mixed condition is equivalent to the most stringent criterion that has so far been established as distinguishing between well- and poorly formulated models. Physically, it implies that a passive tracer uniformly mixed over the full domain remains uniformly mixed at all times. Therefore, if, at some time t_0, the probability density distribution P of positions and velocities of passive tracers is proportional to P_E, the Eulerian joint pdf of position and velocity (i.e., well mixed), then, according to the well-mixed condition, P must remain proportional to P_E at all later times $t > t_0$.

For a given Eulerian flow, the deterministic terms a_i in the LS model can be constrained, but in general not determined uniquely, by the Eulerian statistics of the flow. This nonuniqueness can manifest itself as a ''spin'' term, a_i', that induces a mean rotation of the Lagrangian turbulent velocity vector (Borgas et al. 1997; Sawford 1999; Reynolds 2002a). Models having nonzero mean spin statistics are associated with spiraling particle trajectories, oscillatory velocity autocorrelation functions, and suppressed rates of turbulent dispersion for given turbulent kinetic energies and turbulent kinetic energy dissipation rates. These characteristics are the hallmarks of coherent flow structures such as eddies and vortices. The spin term therefore provides a means of incorporating, into the modeling framework, the effects of en-

ergetic coherent structures seen in Lagrangian and satellite data.

The simplest application of the well-mixed condition is to isotropic, homogeneous, stationary, and incompressible turbulence with Gaussian velocity statistics, mean 0, and variance σ^2. The simplest form of the corresponding LS models arises when the spin term is taken to be linear in velocity, so that $a_i' = \epsilon_{ijk}\Omega_j u_k$, where ϵ_{ijk} is the antisymmetric unit tensor and Ω_j are rotational frequencies. These models are given by

$$du_i = -u_i T_L^{-1} dt + \epsilon_{ijk}\Omega_j u_k dt + b_{ij} d\xi_i, \qquad (2)$$

where T_L is the Lagrangian decorrelation time scale and $b_{ij} = \delta_{ij}(2\sigma^2/T_L)^{1/2}$.

The parameters T_L, Ω, and b_{ij} in Eq. (2) are considered independent from u_i, so that the model is fully linear; that is, the stochastic increment is independent from the state of the system. Nonlinearity has not been considered here because the correspondence between data and model in our application does not support the employment of a more complex, nonlinear formulation.

The Lagrangian velocities simulated through Eq. (2) are Gaussian with mean 0 and variance σ^2 and, therefore, exactly consistent with the prescribed Eulerian velocity statistics. For mesoscale ocean dynamics the two-dimensional form of this model can be considered (Reynolds 2002a), for which the horizontal velocity components u and v are orthogonal to the axis of rotation, Ω_3 (hereinafter simply referred to as Ω). The spin term, which is absent in one-dimensional models (i.e., in models in which the velocity components evolve independently from each other), allows for u and v to be coupled during the entire flow evolution, and the coupling is realized through the angular velocity Ω of the fluctuation field. This parameter is related to the mean rotation $\langle ds\rangle = \langle u\, dv - v\, du\rangle$ during a time increment dt, by (Sawford 1999)

$$\Omega = \frac{\langle ds\rangle}{2dt\,\mathrm{EKE}}, \qquad (3)$$

where EKE is the eddy kinetic energy, equal to $(\langle u^2\rangle + \langle v^2\rangle)/2$. The model represented by Eq. (2) has Lagrangian velocity autocorrelation and cross-correlation functions prescribed by

$$R_{uu} = R_{vv} = e^{-t/T_L}\cos(\Omega t) \quad \text{and}$$
$$R_{uv} = -R_{vu} = e^{-t/T_L}\sin(\Omega t). \qquad (4)$$

The autocorrelations, R_{uu} and R_{vv}, have pronounced negative lobes (i.e., the first negative lobe is more pronounced than the first positive lobe), and, as a consequence, transport is subdiffusive at intermediate times. This means that, for $t \approx T_L$, the associated mean particle dispersion $\langle x^2\rangle$ is proportional to t^α, with $\alpha < 1$—that is, it grows slower than in a typical diffusive process (for equal σ^2 and T_L) given by Taylor's hypotheses (Taylor 1921).

A similar subdiffusive pattern in the velocity autocorrelation functions can be produced by a one-dimensional, second-order model (Berloff and McWilliams 2002). However, such a model cannot reproduce oscillatory cross-correlation functions, R_{uv} and R_{vu}, of the kind represented in Eq. (4), because it does not take into account the correlation in time between orthogonal velocity components. Furthermore, the one-dimensional second-order model cannot produce spiraling trajectories.

The two-dimensional model of Eq. (2) and its corresponding statistics given by Eq. (4) are based on the assumption that the effects of eddy structures can be represented by fixed parameters σ^2, T_L, and Ω. Recent numerical simulations of particle trajectories (Reynolds 2002a) and studies of dispersion processes in idealized models of oceanic gyres (Berloff and McWilliams 2003) have suggested, however, that the particle diffusion can be predicted more realistically by Lagrangian models whose parameters are random variables distributed according to a specified probability density function. In particular, Reynolds (2002a) found that an appropriate choice of this probability distribution can reproduce subdiffusive and superdiffusive features in the Lagrangian autocorrelation functions.

In this paper, we investigate what kind of Lagrangian stochastic model and associated parameter distribution is most suitable to describe the observed float trajectories in the northwest Atlantic. The simplest distribution capturing the coexistence of loopers and nonloopers is a bimodal distribution. A more general trimodality hypothesis would be required if cyclonic and anticyclonic loopers are to be distinguished.

3. Data and methods

a. The float dataset

The dataset analyzed in this paper is archived at the Subsurface Float Data Assembly Center (WFDAC) at Woods Hole. The data span the period from the late 1970s to 1994 and are composed of a number of experiments whose details and related references are listed in Table 1.

Acoustically tracked isobaric floats in the northwestern Atlantic Ocean at the main thermocline level, that is, at a nominal depth of 700 m, have been considered. We chose not to include the isopycnal float data because we did not intend to mix the effects of the isobaric and isopycnic observations within the statistical analyses. Besides, not enough isopycnal data were available for a possible comparison of statistical results from the two datasets. Except for the isopycnical floats and the data from the Topographic Gulf Stream Experiment (TOPOGULF) (Ollitrault and Colin de Verdiere 2002a,b), the Lagrangian dataset analyzed in this paper is similar to that used for past investigations by a number of authors (e.g., Owens 1991; Richardson 1993; Rupolo et al. 1996; Bracco et al. 2000; LaCasce 2000).

TABLE 1. List of SOFAR/RAFOS float experiments in the northwest Atlantic from which the present statistical results were drawn.

Expt	Reference
Abaco Basin	Leaman and Vertes (1996)
Eastern Basin	Spall et al. (1993)
Gulf Stream	Schmitz et al. (1981)
Gulf Stream Recirculation	Owens (1984)
Iberian Basin	Rees and Gmitrowicz (1989)
IFM Iberian Basin	Zenk et al. (1992)
LDE	Rossby et al. (1986)
MODE	Rossby et al. (1975)
Newfoundland Basin	Schmitz (1985)
North Atlantic Tracer Release	Sundermeyer and Price (1998)
Northeast Atlantic	Klein and Mittelstaedt (1992)
Pre-LDE	Riser and Rossby (1983)
Ring	Cheney et al. (1976)
Site L	Price et al. (1987)
Subduction 1991	Sundermeyer and Price (1998)
Topographic Gulf Stream	Ollitrault and Colin de Verdiere (2002a,b)

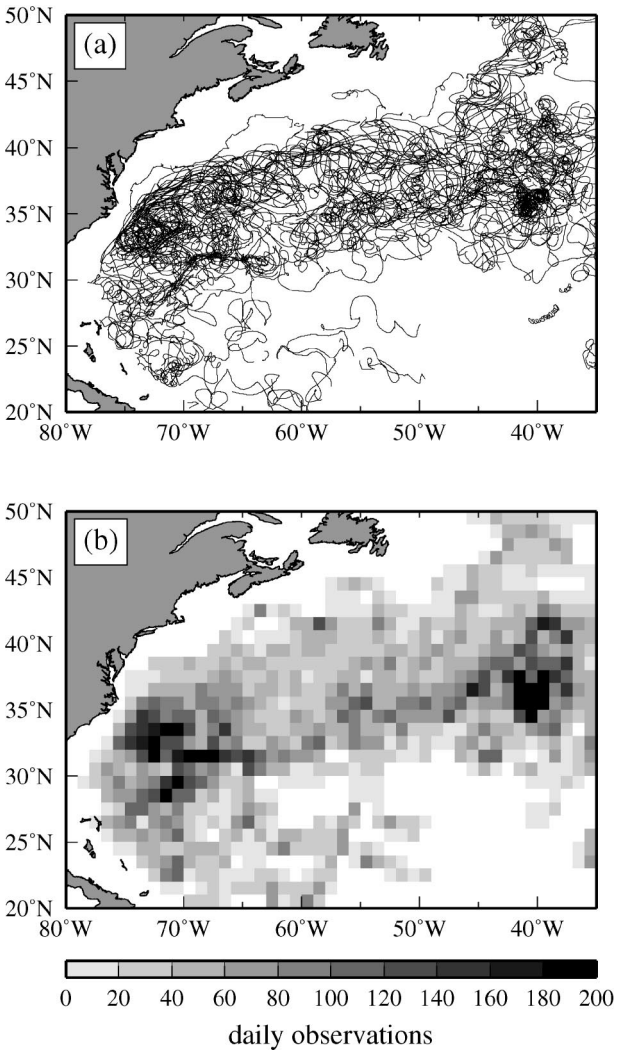

FIG. 1. (a) Spaghetti plot of the acoustically tracked isobaric floats available in the northwestern Atlantic at 700-m depth. (b) Number of daily observation per 1°-square bin of the same dataset.

Float positions were mostly recorded daily. Whenever a different recording time step was used, the velocities were either interpolated or averaged to yield daily observations. The ''spaghetti'' plot of the trajectories, together with the number of observations per 1°-square bin is shown in Figs. 1a and 1b, respectively. The average data density in the Gulf Stream extension is ≈100 days per bin, while it decreases to 50–60 days farther downstream. Higher concentrations, ranging between 150 and 400 days per 1° × 1° box, are found southeast of the jet bifurcation and in the recirculation area southwest of the Gulf Stream.

b. Basin-scale statistics: Estimates of mean flow and eddy kinetic energy

The usual first task when analyzing Lagrangian data is to determine an accurate estimate of the mean flow **U**. The mean flow can be estimated in either an Eulerian or a Lagrangian framework. Following what has been historically done (e.g., Davis 1991), and given that the northwest Atlantic can be characterized by regions with quasi-homogeneous statistical properties, we choose to use an Eulerian-based estimate for the mean flow (also because the way to best estimate a Lagrangian-based mean field remains an open question). The float velocities are then averaged or interpolated to yield an Eulerian distribution in space and time of the mean circulation (''pseudo-Eulerian'' field). A commonly used method is the ''binning technique'' (e.g., Poulain and Niiler 1989; Owens 1991), through which the float velocities are averaged over small spatial subregions (bins) and over a certain period of time. Alternative methods for computing the mean flow can be used, involving objective mapping (Davis 1998) or bicubic spline interpolation (Bauer et al. 1998). The ''eddy'' field is estimated as the residual fluctuation **u** with respect to the estimated mean flow, and as such it includes different kinds of fluctuation phenomena, like vortices due

to flow instabilities, wave fluctuations, and possible seasonal-to-interannual variability.

In this work, the estimate of the mean flow was accomplished through both the bin averaging and the spline interpolation technique. The first method was applied at basin scale over the whole northwest Atlantic region, while both methods have been applied and compared in the more detailed studies of the quasi-homogeneous subregions (section 3c). The statistical results shown in section 4 are based on the spline-interpolated mean field. In all cases, the average was performed over the complete dataset in time, since there are not enough data to resolve nonstationarities at the seasonal or interannual level. This is of course a limitation of the present study, and many more data will be needed in the future to significantly address nonstationary statistics.

The basin-scale investigation was carried out by first changing the bin size in order to test the sensitivity of the results. A 1° × 1° binning was finally chosen as good tradeoff between the importance of resolving both spatial shears of the mean flow and eddy scales on the order of the internal Rossby radius of deformation, and the necessity of keeping a high enough data density per bin to guarantee statistical significance of the results. The binned mean flow and the eddy kinetic energy (EKE) fields are presented in Figs. 2a and 2b, respectively, for bins with a number of independent measurements, n^*, higher than 10. The value of n^* was computed as $n\Delta t/2T_L$, where n is the total number of daily observations, Δt is the sampling interval and T_L is assumed to be ≈10 days (Riser and Rossby 1983; Owens 1991).

The mean circulation (Fig. 2a) shows a strong subsurface Gulf Stream system, with typical averaged velocities of 50 cm s^{-1} beyond Cape Hatteras and 20–30 cm s^{-1} farther downstream. A North Atlantic Current of 30–40 cm s^{-1} is also present around 44°N, 43°W. A pronounced Gulf Stream recirculation is found between 76° and 65°W, together with recirculation gyres south of the stream, approximately centered at 36°N, 62° and 53°W. These results are comparable to similar analyses performed by Owens (1991).

Sources of errors for the mean flow estimates include measurements errors, inaccuracies associated with the fact that velocities are computed from the observed float positions, and sampling errors related to the finite number of data available. The latter are by far the most relevant, and they can be quantified as (Riser and Rossby 1983; Davis 1991)

$$\mathrm{Er}_U = (\sigma_u^2/n^*)^{1/2}, \tag{5}$$

where σ_u^2 is equal to $\langle u^2 \rangle$ (similarly, the subscript v is used for the meridional velocity component). The sampling error of the binned mean flow in Fig. 2a is higher in those regions of the ocean interior and eastern basin where velocities are weak and the data density is low. More quantitative error estimates will be given in section 4 within the discussion of the regional analysis. Other error sources are the biases due to gradients in the data spatial distribution and gradients in eddy diffusivities (Davis 1991; Freeland et al. 1975). They are typically smaller than the sampling errors and are considered negligible for the purposes of this work (Garraffo et al. 2001a).

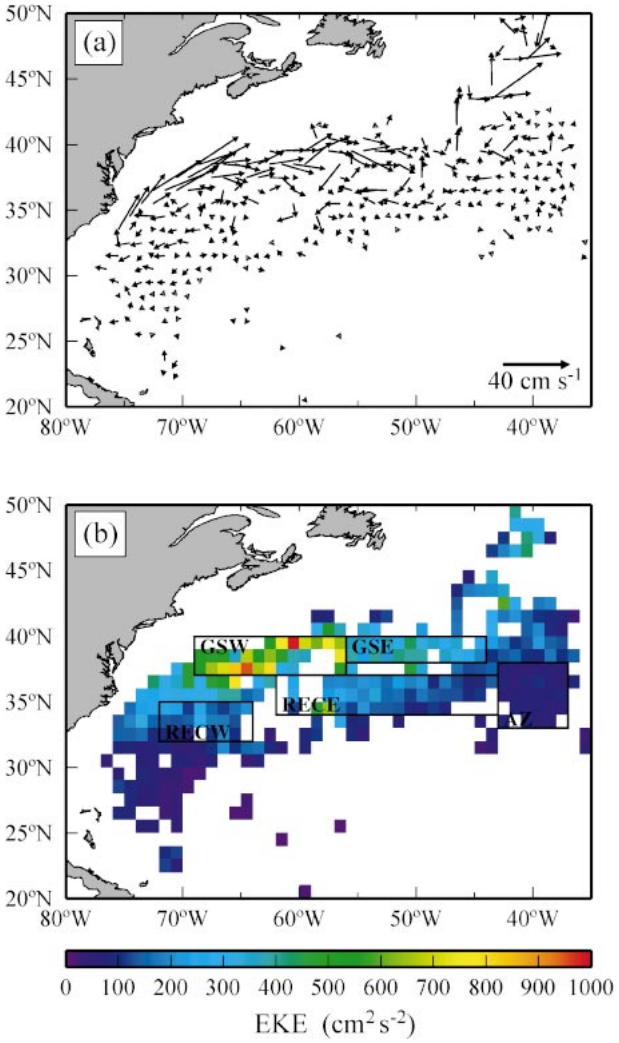

FIG. 2. (a) Binned mean velocity field obtained by averaging the 700-m float data over 1° × 1° bins. (b) Binned eddy kinetic energy field and contours of the five subregions where detailed data analyses have been carried out.

The eddy kinetic energy distribution (Fig. 2b) shows the highly energetic region of the Gulf Stream extension, with EKE ≈ 800 cm^2 s^{-2} around 38°N, 65°W. The rest of the basin has much lower eddy variability, with typical interior EKE ≈ 50 cm^2 s^{-2}. The sampling error of the eddy kinetic energy field can be estimated as

$$\mathrm{Er}_{\mathrm{EKE}} = \left[\frac{\sigma_u^4 + \sigma_v^4}{2(n^* - 1)}\right]^{1/2}. \tag{6}$$

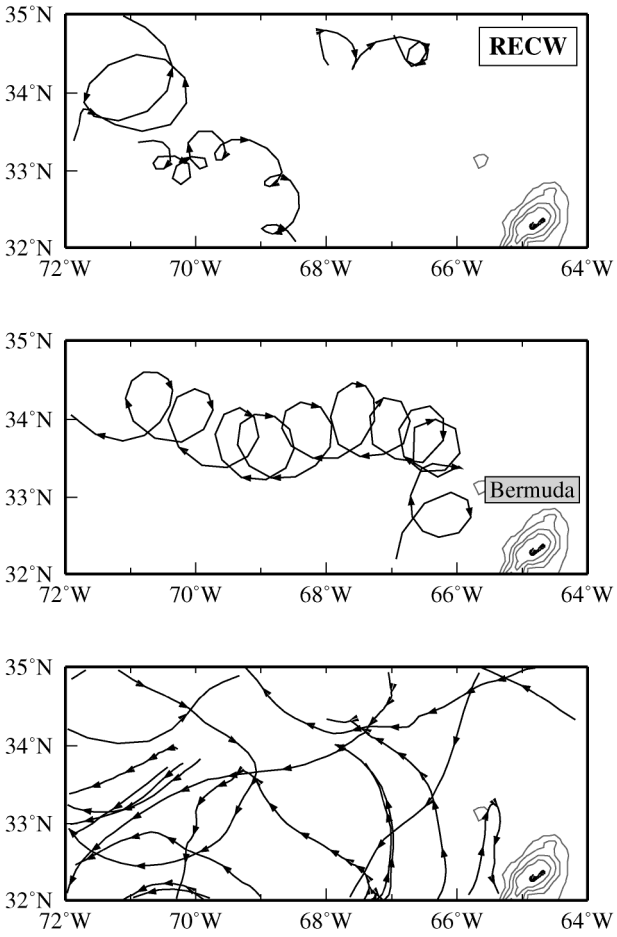

FIG. 3. Sample of (top), (middle) loopers and (bottom) nonloopers in the recirculation region RECW. Arrows along the trajectories are plotted every 5 days.

Our 1° × 1° binned EKE field has typical errors between 20% and 30%.

c. Quasi-homogeneous regions

In Fig. 2b, superimposed on the distribution of eddy kinetic energy, are the contours of five subregions where we have focused our study of the mesoscale turbulent field. These areas are characterized by quasi-homogeneous eddy kinetic energy levels, in order to identify regions that are approximately statistically homogeneous. The two areas named GSW and GSE (Gulf Stream west and east, respectively) are the most energetic, with eddy kinetic energy ranging between 300 and 800 $cm^2\ s^{-2}$, and are located in the Gulf Stream extension between 69° and 44°W. Regions RECW and RECE (Recirculation west and east) are the recirculation areas southwest and south of the jet axis. They are characterized by relatively weaker EKE levels (50–200 $cm^2\ s^{-2}$). Last, region AZ (for the Azores Current) is located southeast of the Gulf Stream bifurcation and has eddy energy lower than 50 $cm^2\ s^{-2}$.

TABLE 2. Number of total Lagrangian data, nonlooping, and looping trajectory data in float days, for each region of the northwestern Atlantic Ocean. The loopers percentage is also in terms of days.

			Loop			
REG	Tot	No loop	Cycl	Acycl	Tot	Loop (%)
RECW	2253	1917	127	209	336	15
RECE	3797	2738	966	93	1059	28
GSW	1339	979	283	77	360	27
GSE	1155	946	182	27	209	18
AZ	3554	2134	1195	225	1420	40

In addition to the energy characterization, these regions also exhibit different dynamical regimes. GSW and GSE are dominated by the Gulf Stream jet, a highly coherent and nonlinear structure that limits cross transport and mass exchanges. Float trajectories tend to be advected out of the area within time scales shorter than 30 days. The recirculation regions RECW and RECE are dominated by highly energetic eddies and Gulf Stream rings, because of the instability processes and nonlinear dynamics typical of this part of the ocean. Region AZ is also eddy dominated, but the characteristic energy of the vortices is significantly lower than that found in the Gulf Stream recirculation area.

The direct effect of coherent structures, such as rings, submesoscale coherent vortices, and large-amplitude meanders, is to produce two distinct categories of float trajectories (Richardson 1993). The loopers are the quickly rotating floats that are trapped inside highly energetic eddies, while the nonloopers represent the rest of trajectories, which experience little looping behaviors, and are typically associated with the less energetic background flow. Richardson (1993) has introduced a simple criterion of defining a looper as a trajectory that undergoes at least two consecutive loops in the same direction. This same criterion has been adopted here as initial identification method. Furthermore, in the few cases in which a float stopped looping (i.e., when it stopped being influenced directly by the coherent structure) the subsequent part of the trajectory has been considered as nonlooper. A sample of looping and nonlooping trajectories found in region RECW (Gulf Stream recirculation) is shown in Fig. 3.

A more quantitative method of looper identification, based on LS parameter estimation, has also been used (see section 5), in order to take into account looping trajectories that do not exhibit a clear spiraling behavior (because of temporary weakening of the vortex they are embedded in, or because they are influenced by strong background flows, e.g.).

The distribution of loopers and nonloopers resulting from this criterion, in number of float days, and for each region, is presented in Table 2. The highest percentage of looping floats is found in region AZ (southeast of the Gulf Stream bifurcation, slightly west of the Mid-Atlantic Ridge), where a number of trajectories were embedded in fairly steady vortices. Some of the loopers

in GSW and GSE (Gulf Stream axis) are in meanders, and it is not clear whether they are merely following the jet and its local recirculation gyres or they were trapped in Gulf Stream rings and were subsequently ejected. The total number of float days in all the five subregions is 12 098. Out of these, 3384 days (28%) are from looping trajectories. The percentage is slightly higher than the 21% given by Richardson (1993), probably because the more recent TOPOGULF experiment float data were not included in Richardson's analysis and these floats contribute to the number of loopers in region AZ.

d. Mean flow estimates in the quasi-homogeneous regions

In the subregions, the statistical analysis of the residual velocity **u** has been carried out by computing autocovariance and cross-covariance functions (section 4). Since **u** was determined by subtracting the mean flow **U** from the total Lagrangian velocities, an important prerequisite to the analysis is that the results are independent of the averaging scales and of the method used to compute **U**. This has been verified in a preliminary investigation, in which the two methods of binning and spline interpolation have been applied and compared in each region. Notice that, with respect to the binning, the bicubic spline interpolation (Bauer et al. 1998) has the advantage of providing a continuous space-dependent mean flow, so that large-scale horizontal shears can be directly taken into account. Furthermore, Lagrangian statistics are expected to be evaluated more accurately, since the separation between mean and eddy field is performed continuously for each trajectory point.

To test the robustness of the eddy statistics with respect to the **U** estimates, we have performed an extensive sensitivity investigation by varying the parameters that characterize the spline-interpolated field (see appendix A). It has been found that, for all the spline parameter choices, the eddy statistics tend to behave asymptotically at high values of roughness ρ (see appendix A for definitions), with the autocovariance and cross-covariance structures becoming independent from the specific value of ρ. A further comparison has been carried out with the results obtained by using the binned mean flow, showing that the same features of the eddy field are reproduced. This suggests that the mean flow shear is correctly resolved, within the limits of the present float data coverage, and that the **u** statistics are robust, independent from the specific estimates of **U**.

4. Lagrangian statistical analysis

In this section, the turbulent residual velocity **u** is analyzed in the various subregions, computing autocovariance and cross-covariance functions from the overall Lagrangian dataset, and separately from the looper and the nonlooper datasubsets. Both methods of looper identification have been used, the Richardson criterion and the quantitative method described in section 5, although no noticeable differences in the results have been observed.

a. Gulf Stream recirculation region (RECW)

Region RECW (Fig. 2b) is located at the western edge of the Gulf Stream recirculation and is dominated by an eastward recirculation mean flow of 2.7 ± 0.9 cm s^{-1}. The standard error is computed from Eq. (5) by using the zonal variance σ_u^2 and $n^* = 187$, obtained using an a posteriori choice of the Lagrangian time scale equal to 6 days (see subsequent parameter estimation for details). The overall eddy kinetic energy is 142.3 ± 10.4 $cm^2 s^{-2}$, where the sampling error is estimated from Eq. (6). The correspondent root-mean-square velocity, $V_{rms} = (2EKE)^{1/2}$, is 16.7 cm s^{-1}, which indicates that the fluctuation field is significantly more energetic than the mean flow.

The majority of subsurface Lagrangian data present in this region are from SOFAR floats released at 700-m nominal depth during the Site L Experiment (Price et al. 1987), and in the Local Dynamics Experiment (LDE; Rossby et al. 1986). Most of the floats (80%) leave the region in less than 40 days, whereas some of them, typically the looping floats, remain trapped in the area for 3–6 months. Anticyclonic looping trajectories dominate over the cyclonic ones in terms of days (Table 2). They may be due to the presence of anticyclonic subsurface warm lenses whose formation has not been completely clarified yet. Possible explanations involve the separation of 18°C water patches from the Gulf Stream (Brundage and Dugan 1986) and interactions with the Corner Rise seamounts at 36°N, 52°W (Richardson 1980).

The autocovariance and cross-covariance functions from the overall data in RECW and from the separated datasets of the nonloopers and anticyclonic looping floats are shown in Figs. 4 and 5, respectively. The results obtained from the cyclonic floats are too noisy because of the small amount of cyclonic data and are not displayed here. The 95% confidence limit (CL) is also plotted. For the autocovariance case, this is estimated as $2\sigma^2/(n^*)^{1/2}$ (Priestley 1981). For the cross-covariance case, the 95% CL is computed as $2[(\sigma_u^2\sigma_v^2 - \sigma_{uv}^2)/n^*]^{1/2}$ (Sciremammano 1979), where σ_{uv}^2 is the squared cross covariance at 0 time lag ($\langle uv \rangle$).

The overall autocovariance function (Fig. 4a) exhibits a strong oscillation pattern, with a significant positive lobe that is more pronounced than the first negative lobe. This behavior is representative of ''superdiffusion'' processes because the associated eddy dispersion grows faster than the typical diffusive spreading, at intermediate times ($\langle x^2 \rangle \propto t^\alpha$, with $\alpha > 1$, for $t \approx T_L$). A similar outcome was obtained by Berloff et al. (2002) in their numerical simulations of the mesoscale transport dis-

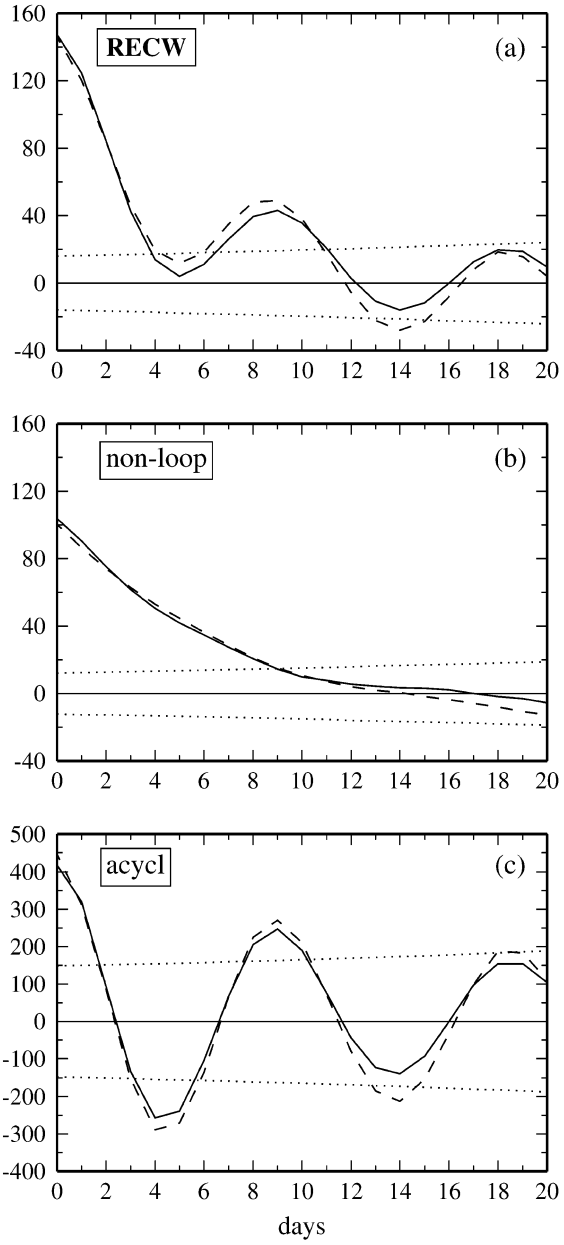

FIG. 4. Zonal (solid line) and meridional (dashed line) velocity autocovariance functions ($cm^2\ s^{-2}$) computed in the recirculation region RECW from (a) the overall dataset and separately from (b) the nonloopers and (c) the anticyclonic looping trajectories. The dotted lines denote the 95% CL.

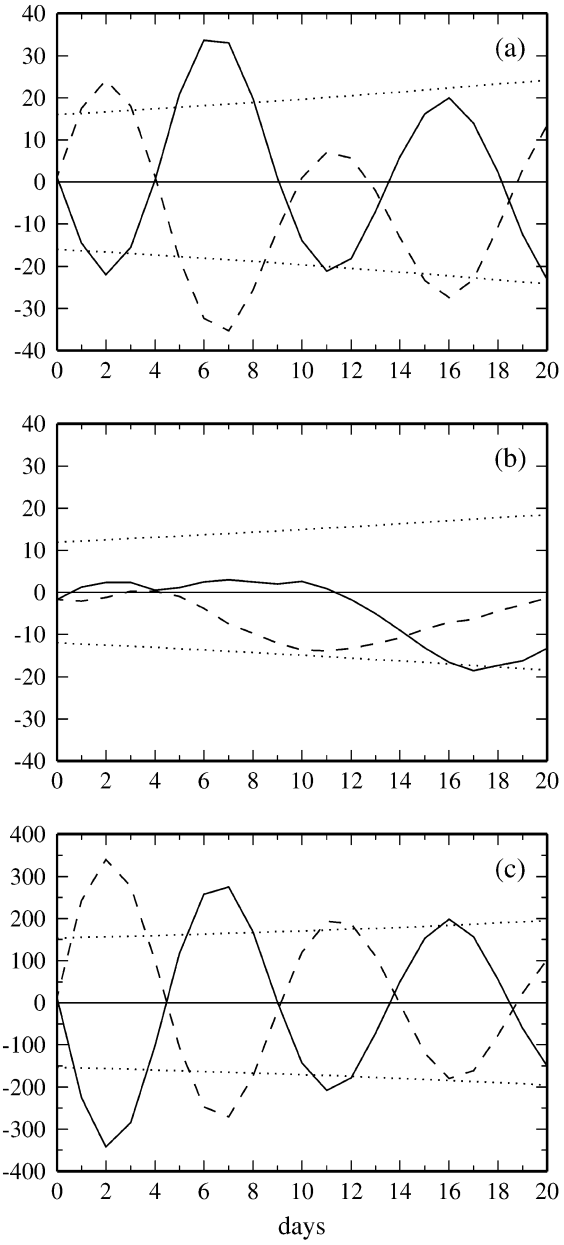

FIG. 5. Velocity cross-covariance functions (R_{uv} and R_{vu}, plotted as solid and dashed lines, respectively), computed in RECW from (a) the overall Lagrangian data and separately from (b) the nonloopers and (c) the anticyclonic loopers. The 95% CL is drawn again as dotted lines. The *y*-axis units are centimeters squared per second squared.

tribution in a double-gyre model. They analyzed the autocorrelation and dispersion functions in different regions of the western boundary current extension and subtropical gyre, providing a complete description of the eddy variability for an idealized ocean. In particular, the velocity autocorrelation functions in their central subtropical gyre show superdiffusive behaviors that are qualitative very comparable with our results (see Fig. 10 in Berloff et al. 2002). In a companion paper, Berloff and McWilliams (2002) applied higher-order Lagrangian stochastic models to describe these anomalous features of the eddy field.

In the present work, we suggest that the ''superdiffusivity'' arises from the superposition of the two different eddy regimes described by the nonlooping and looping floats. In terms of autocovariance functions, this is clear in Fig. 4, where the nonloopers give rise to an exponentially decaying velocity autocovariance (Fig.

4b) that, when superposed onto the oscillatory autocovariance function obtained from the anticyclonic floats (Fig. 4c), yields the overall results shown in Fig. 4a. The nonlooping trajectories are associated with an eddy kinetic energy of ≈ 100 cm^2 s^{-2} ($V_{\rm rms} \approx 14$ cm s^{-1}) and are characterized by a Lagrangian decorrelation time scale $T_L \approx 7$ days. The anticyclonic loopers are representative of a more energetic eddy field than that described by the nonloopers, exhibiting EKE levels on the order of 400 cm^2 s^{-2} ($V_{\rm rms} \approx 29$ cm s^{-1}). They also feature a longer decorrelation scale ≈ 12 days and an oscillation time scale $T_w \approx 10$ days.

The coexistence of two separate eddy regimes is further shown by the results in terms of velocity cross-covariance functions. In this case, the pattern of the overall statistics depicted in Fig. 5a indicates a strong contribution of the oscillating cross covariances associated with the anticyclonic loopers (Fig. 5c), while the cross-covariance functions obtained from the nonlooping floats (Fig. 5b) are not significantly different from zero.

The scenario can be summarized as follows. The nonloopers are representative of a background flow field whose instantaneous velocities decorrelate exponentially with time, each component independently from each other. The looping trajectories give rise to oscillations in both the autocovariance and cross-covariance functions, indicating that they are affected by a rotating eddy velocity field that is more energetic than the background eddy regime.

The oscillatory pattern in the looper statistics resembles the behavior dictated by Eq. (4), suggesting that the eddy features can be reproduced by a two-dimensional, first-order Lagrangian stochastic model of the kind described by Eq. (2) with a finite value of spin, Ω. Similar oscillatory features in the autocovariance function are also predicted by a one-dimensional, second-order model that was applied by Berloff and McWilliams (2002). This model reproduces the oscillatory subdiffusive behavior in the autocovariances by introducing appropriate time scales for the acceleration field, but it does not exhibit oscillatory cross-covariance functions typical of rotating coherent structures. One-dimensional LS models are therefore not suitable to describe our statistical results for the loopers in RECW and in the other regions of the northwestern Atlantic.

The two-dimensional model of Eq. (2) can be used to interpret the nonlooper statistics as well, by adopting $\Omega = 0$ in the model equations. Therefore, we hypothesize that the overall statistical behavior can be represented by a two-dimensional, first-order LS model with a bimodal distribution of spin, that is, with distinct values of spin associated with the nonlooping and looping trajectories. More generally, we should consider trimodal distributions of spin, since we associate positive (negative) values of Ω to cyclonic (anticyclonic) loopers. However, each region is characterized by a dominant sign of angular velocity, and for this reason we will mostly refer to the bimodality hypothesis. The probability associated with each family of trajectories is dictated by the actual data distribution (percentage of loopers in Table 2).

To test the applicability of the model represented by Eq. (2), the parameters σ^2, T_L, and Ω are estimated from the looper and nonlooper datasubsets, and simulations of numerical trajectories are carried out by integrating Eq. (2) with the estimated parameters. The statistics obtained from the simulated trajectories are compared with the autocovariances and cross covariances computed from the real floats.

The method used to estimate the model parameters is described in appendix B. Here we concentrate on discussing the results that are reported in Table 3. We notice that RECW is characterized by turbulent dynamics that are nearly isotropic, with comparable zonal and meridional parameters within the limits of the error bar. The angular velocity for the nonloopers is approximately 0, while the anticyclonic loopers have $\Omega \approx -0.54$ days^{-1}, corresponding to an oscillation time scale T_w on the order of 11 days (for the cyclonic loopers $\Omega \approx 0.31$ days^{-1} and $T_w \approx 20$ days). The average vortex radius r computed for the looping floats is approximately equal to 47 (66) km for the anticyclones (cyclones).

The parameters listed in Table 3 are used to numerically integrate Eq. (2) and simulate three groups of trajectories representative of the nonlooping, the cyclonic, and the anticyclonic looping real floats. The number of trajectories and their duration are set in such a way to reproduce the total number of real float days available in each datasubset. From the synthetic trajectories, we carried out similar statistical analyses as performed for the real Lagrangian data. The results in terms of autocovariance functions are shown in Fig. 6 for the overall simulated floats and for the nonlooping and anticyclonic numerical trajectories. The cross-covariance functions are presented in Fig. 7.

The most important outcome is that the autocovariance and cross-covariance functions computed from the combined three groups of simulated floats (Figs. 6a and 7a) are very comparable to the corresponding statistics obtained from all the real data available in region RECW (Figs. 4a and 5a). This means that the Lagrangian stochastic model with the bimodal (trimodal) spin distribution did succeed in reproducing the statistical results that were previously investigated. The major eddy features, such as the superdiffusive characteristic of the overall autocovariance function and the oscillating patterns in both the autocovariances and cross covariances, are predicted by the synthetic trajectories. Furthermore, the statistics from the numerical nonlooping and anticyclonic floats depicted in Figs. 6b,c and 7b,c are also very similar to their counterparts obtained from the real float subsets (Figs. 4b,c and 5b,c, respectively).

TABLE 3. Estimates of the first-order two-demensional Lagrangian stochastic model parameters, in the five subregions of the northwestern Atlantic, for the nonlooping (no loop), the cyclonic (cycl), and the anticyclonic (acycl) trajectory subsets. The computation of the parameters and their errors has been explained in appendix B. The symbols stand for the velocity variance $\sigma^2_{u,v}$ and the decorrelation time scale $T_L^{u,v}$ (subscript/superscript u, v for either zonal or meridional estimates), the rms velocity $V_{\rm rms}$, the angular velocity Ω, the oscillation time scale T_w, and the average radius r, respectively.

	$\sigma^2_{u,v}$ (cm^2 s^{-2})	$V_{\rm rms}$ (cm s^{-1})	$T_L^{u,v}$ (days)	Ω (days^{-1})	T_w (days)	r (km)
RECW						
No loop	103.7 ± 9.8	14.3 ± 0.6	6.8 ± 1.0	0.02 ± 0.01	*O*(300)	*O*(600)
	100.3 ± 13.4		7.9 ± 1.5			
Cycl	278.0 ± 45.0	23.6 ± 2.0	8.0 ± 3.4	0.31 ± 0.05	20.3 ± 3.8	65.7 ± 11.1
	278.0 ± 54.2		8.2 ± 3.7			
Acycl	417.0 ± 79.0	29.4 ± 2.6	12.1 ± 2.5	−0.54 ± 0.06	11.6 ± 1.5	47.0 ± 7.7
	447.0 ± 86.4		12.3 ± 3.4			
RECE						
No loop	163.3 ± 15.5	17.3 ± 0.5	8.3 ± 0.9	0.04 ± 0.01	*O*(150)	*O*(400)
	135.5 ± 5.4		7.0 ± 0.4			
Cycl	234.2 ± 29.0	21.6 ± 1.5	6.5 ± 1.1	0.34 ± 0.04	18.5 ± 2.8	54.8 ± 10.0
	231.8 ± 39.5		7.7 ± 2.0			
Acycl	143.1 ± 37.1	20.4 ± 3.6	6.7 ± 2.8	−0.16 ± 0.06	39.3 ± 26.5	110.3 ± 54.4
	273.8 ± 111.4		14.4 ± 6.8			
GSW						
No loop	741.0 ± 51.8	35.9 ± 1.1	7.8 ± 1.1	0.02 ± 0.01	*O*(300)	*O*(1300)
	550.0 ± 50.2		7.3 ± 1.1			
Cycl	294.0 ± 52.3	24.6 ± 1.9	3.7 ± 0.9	0.21 ± 0.04	30.0 ± 8.1	101.3 ± 28.5
	312.0 ± 49.8		6.7 ± 1.7			
Acycl	200.0 ± 85.2	19.5 ± 3.5	12.8 ± 8.1	−0.16 ± 0.05	39.3 ± 21.3	105.4 ± 59.6
	181.0 ± 62.8		15.3 ± 29.0			
GSE						
No loop	298.0 ± 18.0	24.3 ± 0.7	6.9 ± 0.6	0.06 ± 0.02	*O*(100)	*O*(350)
	294.0 ± 26.6		6.1 ± 0.6			
Cycl	412.0 ± 93.8	26.2 ± 1.9	9.8 ± 2.0	0.39 ± 0.07	16.1 ± 3.5	58.1 ± 12.3
	276.0 ± 89.4		6.6 ± 3.4			
Acycl	440.0 ± 263.1	25.9 ± 8.4	20.3 ± 17.5	−0.47 ± 0.11	13.4 ± 4.8	47.7 ± 10.6
	233.0 ± 164.2		17.2 ± 16.3			
AZ						
No loop	64.6 ± 5.3	11.6 ± 0.3	14.7 ± 1.7	−0.01 ± 0.01	*O*(800)	*O*(1200)
	70.8 ± 3.5		15.3 ± 1.7			
Cycl	67.6 ± 6.8	12.2 ± 0.6	11.1 ± 1.3	0.19 ± 0.02	33.1 ± 4.8	55.4 ± 7.0
	81.0 ± 9.1		7.9 ± 1.0			
Acycl	55.9 ± 14.0	10.6 ± 0.8	15.0 ± 3.6	−0.12 ± 0.02	52.3 ± 16.7	76.3 ± 25.3
	56.5 ± 7.0		15.7 ± 3.1			

b. The other northwest Atlantic regions

1) REGION RECE

This area (Fig. 2b) is located south of the Gulf Stream axis between 62° and 43°W, therefore encompassing the whole recirculation branch of the northern subtropical gyre. It comprises the southern half of the Worthington gyre, while its western part is dominated by a clockwise mean circulation suggesting the presence of another recirculation gyre to the west. The region zonal mean flow is -2.6 ± 0.7 cm s^{-1}, whereas the meridional component is -1.4 ± 0.7 cm s^{-1}, thus forming a west–southwest mean circulation. The eddy kinetic energy is 156 ± 8.8 cm^2 s^{-2}, with a corresponding rms velocity of $\approx$17.7 cm s^{-1}.

Most of the Lagrangian data in this region are 700-m SOFAR floats released during the Gulf Stream Recirculation Experiment (Owens 1984) aimed at giving the first long-term thermocline description of the Gulf Stream and its recirculation dynamics, and floats from TOPOGULF, which investigated the influence of the Mid-Atlantic Ridge on large-scale and mesoscale motions (Ollitrault and Colin de Verdiere 2002a,b). Similar to RECW, 75% of the floats leave the area in less than 40 days, while about 14% of them remain for periods between 2 and 8 months. The total number of independent measurements, n^*, is equal to 316. The number of looping trajectories in RECE constitutes 28% of the total float days (Table 2), and they are mainly cyclonic particles trapped inside Gulf Stream cold rings or in ring–stream interactions. Some loopers are in eddies spawned through interactions with the Corner Rise seamounts, which consist of a cluster of six individual seamounts centered at 36°N, 52°W rising from the ocean floor up to 650-m depth.

The statistical results in terms of autocovariance and cross-covariance functions computed from the overall Lagrangian data and separately from the nonlooping and

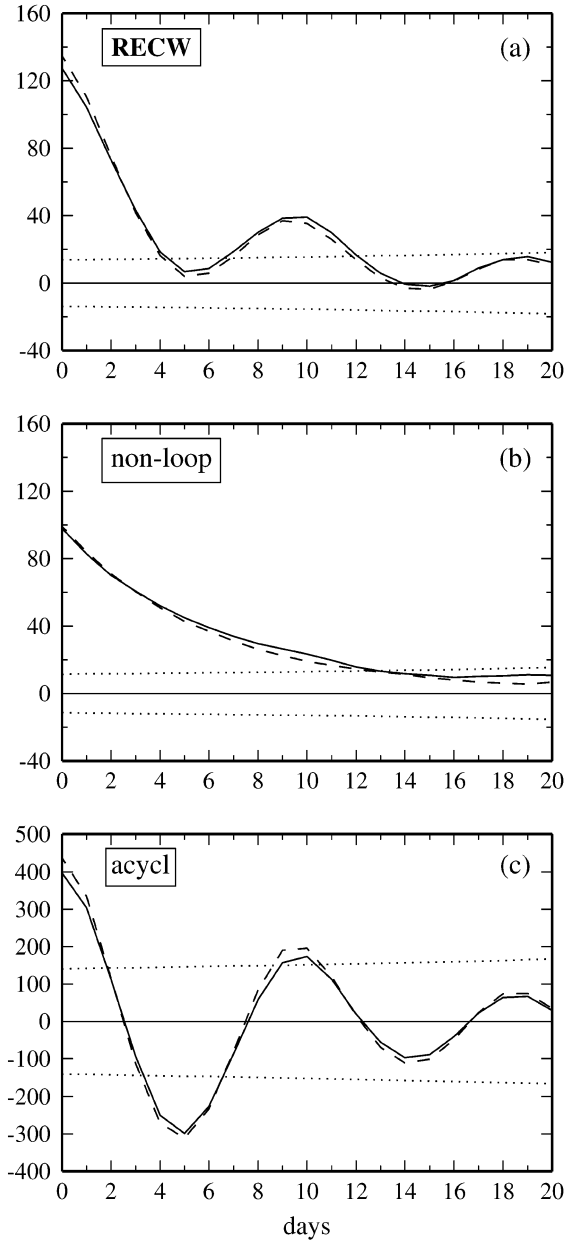

FIG. 6. Velocity autocovariance functions (the different line types are the same as for the previous figures) obtained from the simulated Lagrangian datasets in RECW. Results are from (a) the total synthetic trajectories and from (b) the simulated nonloopers and (c) the anticyclonic loopers, respectively. These modeled statistics must be compared with the results computed from the real data in Fig. 4.

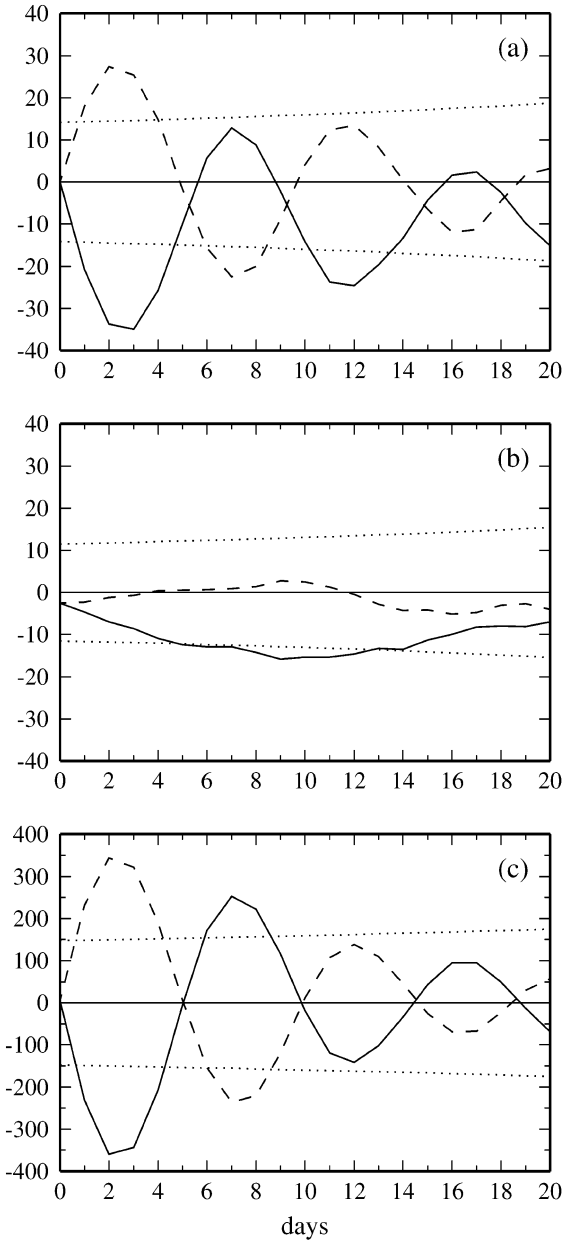

FIG. 7. Same as in Fig. 6, but for the simulated velocity cross-covariance functions. The modeled statistics can be compared with the results obtained from the real data in Fig. 5.

the cyclonic rotating trajectories in RECE are shown in the upper three panels of Figs. 8 and 9 (each panel is clearly identified by text). Hereinafter, only the statistics from the dominating loopers (either cyclonic or anticyclonic) will be displayed for each region.

Similarly to what was found in RECW, this region exhibits oscillating autocovariances with pronounced positive lobes and weaker negative lobes. Despite the fact that some features remain within the 95% confidence limits, a small curve protuberance around 6–7 days does exist, especially in the zonal autocovariance function, which is indicative of a superdiffusive eddy field. Furthermore, the oscillations in the cross-covariance functions are statistically significant, suggesting that the eddy flow characteristics are not too different from those identified in region RECW. Some distinctions arise, however, in the statistics obtained from the cyclonic looping trajectories (right upper panel in both Figs. 8 and 9). Unlike the straight oscillatory autocovariance and cross-covariance functions calculated for

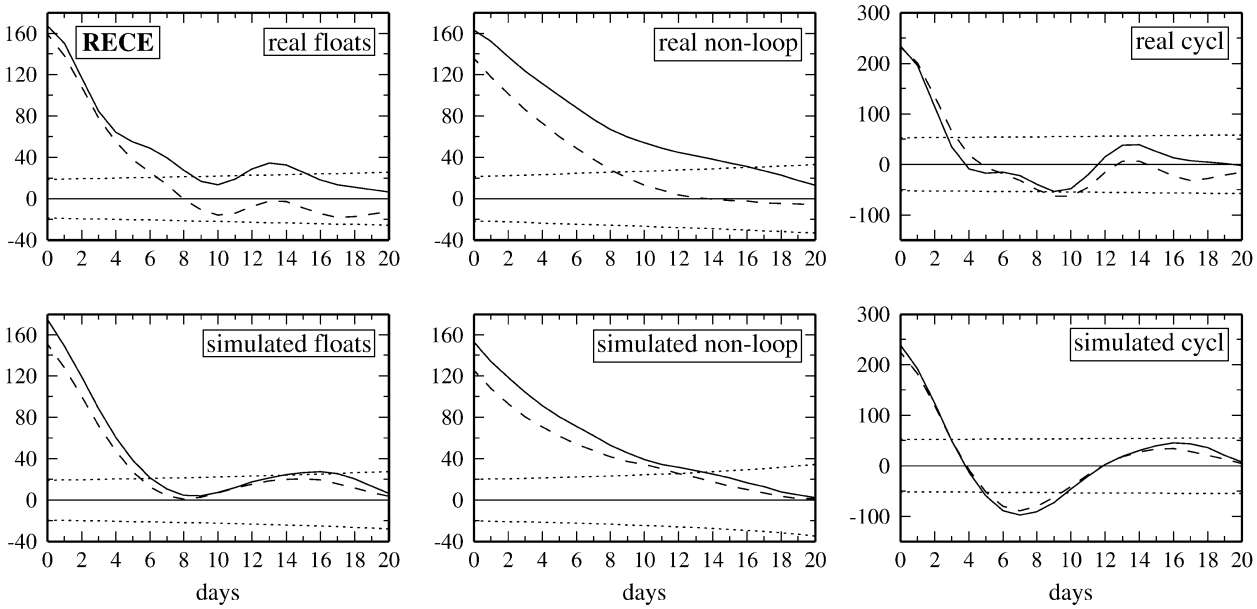

FIG. 8. Velocity autocovariance functions computed in the recirculation region RECE. (top) Results from (left) the real overall Lagrangian data, (middle) the nonlooping floats, and (right) the cyclonic looping floats. (bottom) Results from (left) the simulated total trajectories, (middle) the synthetic nonloopers, and (right) the cyclonic loopers. Direct comparisons can be made between the real and the modeled statistics by comparing the top panels with the bottom panels.

the looping floats of RECW, the RECE statistics show a more complex behavior suggesting the presence of various coherent structures with different spatial and rotational time scales. This point will be further developed and discussed in section 5.

By continuing to assume a simple bimodality hypothesis in this region, we test the applicability of a first-order Lagrangian stochastic model with different values of spin to be attributed to the nonlooping and looping floats. The model parameters are computed from the real Lagrangian data as for RECW (Table 3). We notice that the oscillation time scale T_w is slightly longer than the one resulting from the anticyclonic loopers of region RECW (18 vs 11 days), while the nonrotating floats continue to exhibit approximately 0 angular velocity. Similarly to what was performed for RECW, we

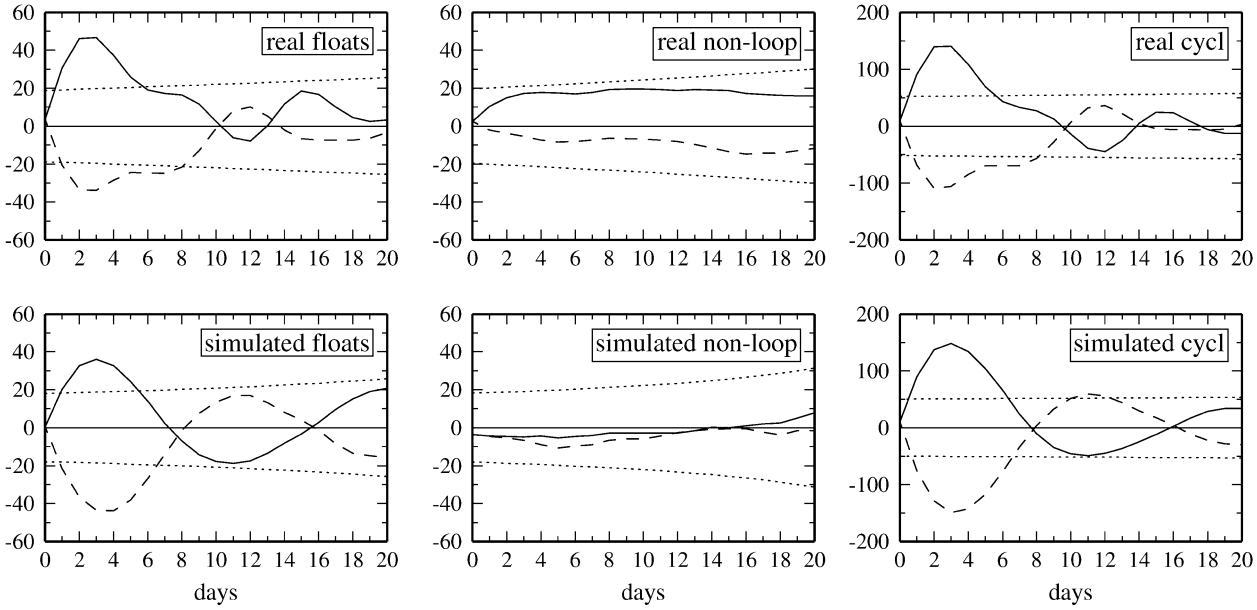

FIG. 9. Same as in Fig. 8, but for the velocity cross-covariance functions.

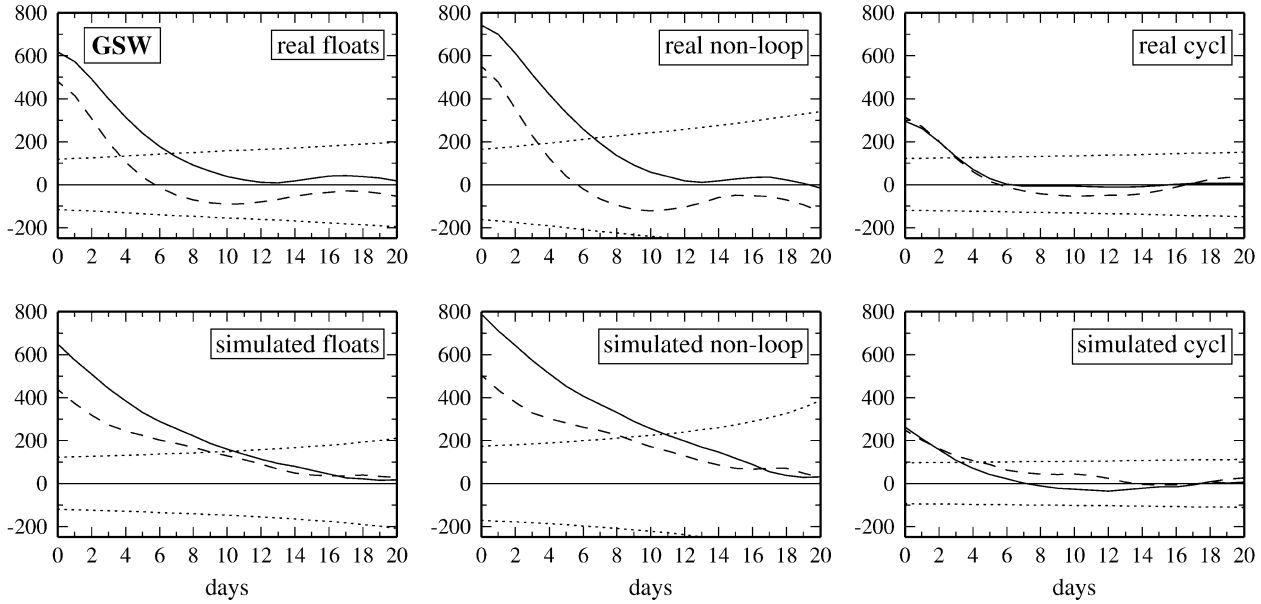

FIG. 10. Velocity autocovariance functions determined in the Gulf Stream extension region GSW, as in Fig. 8.

used these parameters to numerically integrate Eq. (2) and simulate three groups of trajectories representative of the real nonloopers, cyclonic loopers, and anticyclonic loopers. The autocovariance and cross-covariance functions obtained from the synthetic trajectories are displayed in the lower panels of Figs. 8 and 9. The main oscillation patterns of these statistics for the overall real floats (left upper panel in Figs. 8 and 9) are clearly reproduced by the synthetic trajectories, although the detailed structure appears different and less smooth than that predicted by the simulations. This is presumably due to coherent structures characterized by various scales not entirely represented by the single Ω and T_L of the simulated cyclones.

2) REGIONS GSW AND GSE

The two regions (Fig. 2b) are the most energetic areas of the northwestern Atlantic because they are located along the Gulf Stream axis. GSE is the eastward continuation of GSW and extends slightly east of the jet bifurcation where the Gulf Stream starts flowing northward as North Atlantic Current. Both regions are characterized by a mainly eastward mean flow, equal to 12 $\pm$ 2.4 cm s^{-1} in GSW and to 6.3 $\pm$ 1.8 cm s^{-1} in GSE (with nonsignificant mean meridional component). The eddy kinetic energy reaches 547.7 $\pm$ 52.6 cm^2 s^{-2} in GSW, corresponding to a rms velocity of $\approx$33 cm s^{-1}, while the eddy energy level is lower in GSE and equal to 304.3 $\pm$ 31.3 cm^2 s^{-2} ($V_{\text{rms}} \approx 25$ cm s^{-1}). As expected, the two regions are characterized by stronger mean circulation and higher eddy kinetic energy than those found in the recirculation areas RECW and RECE analyzed previously. However, the fundamental difference between the Gulf Stream and the recirculation regions lies in the dynamics, since GSW and GSE are dominated by two kinds of coherent structures, the jet meanders and the Gulf Stream rings that are shed in response to the current instabilities. The Lagrangian data are affected by both types of coherent features, and consequently their eddy statistics contain the effects of the unstable jet and the oscillating characteristics due to the rotating vortices.

Most of the floats in GSW and GSE are from the Gulf Stream Recirculation and the Site L experiments. About 85% of them leave the regions in less than 30 days, the majority being advected quickly away by the strong Gulf Stream current. The looping trajectories tend to rotate mainly in the counterclockwise direction, although they may not correspond always to cyclonic eddies. In region GSW, for example, some loopers are waving and moving with the jet, and it is difficult to discern whether the rotation is due to the trapping action of semidetached rings or to the fluctuation of the meandering jet. In region GSE, rotating vortices are more easily recognizable and are possibly due to Gulf Stream cold rings. The total number of independent measurements is 111 and 96 for GSW and GSE, respectively.

The autocovariance and cross-covariance functions computed in region GSW are displayed in the upper three panels of Figs. 10 and 11. The same statistics for GSE are shown in the upper panels of Figs. 12 and 13. In region GSW, the autocovariance functions for the overall float data seem to be dominated by the nonlooping trajectories (left and middle upper panels in Fig. 10). Furthermore, the turbulent field associated with the cyclonic floats is less energetic than that represented by the remaining trajectories. The results suggest that the anomalous behavior of the overall statistics is not only

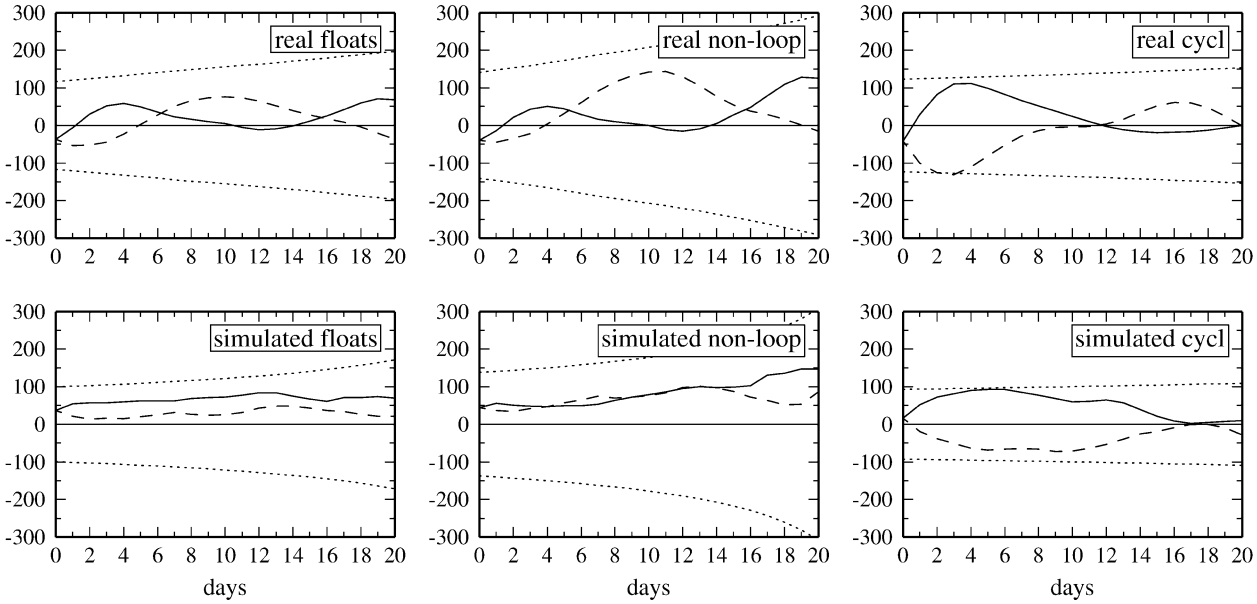

FIG. 11. Same as in Fig. 10, but for the velocity cross-covariance functions.

due to the looper's influence, but also to the effect of additional eddy mechanisms such as jet meanderings or fluctuations of the mean field. These assertions, however, are merely speculative, since the oscillations of both the autocovariance and cross-covariance functions remain within the 95% CL. The situation is simpler in region GSE where the superdiffusive autocovariance obtained from the complete float dataset (left-upper panel in Fig. 12) seems once again the result of the superposition of the statistics computed from the nonloopers and the cyclonic looping trajectories (middle and right upper panels in the same figure). A common feature of GSW and GSE is that the loopers and the nonloopers exhibit comparable eddy kinetic energy levels, indicating the presence of a background flow field as energetic as the rotating coherent structures.

The estimate of the parameters derived by assuming the applicability of a first-order, two-dimensional Lagrangian stochastic model in GSW and GSE is again reported in Table 3. The rms velocities of the looping floats are slightly higher than those characterizing the loopers of the recirculation regions RECE and RECW.

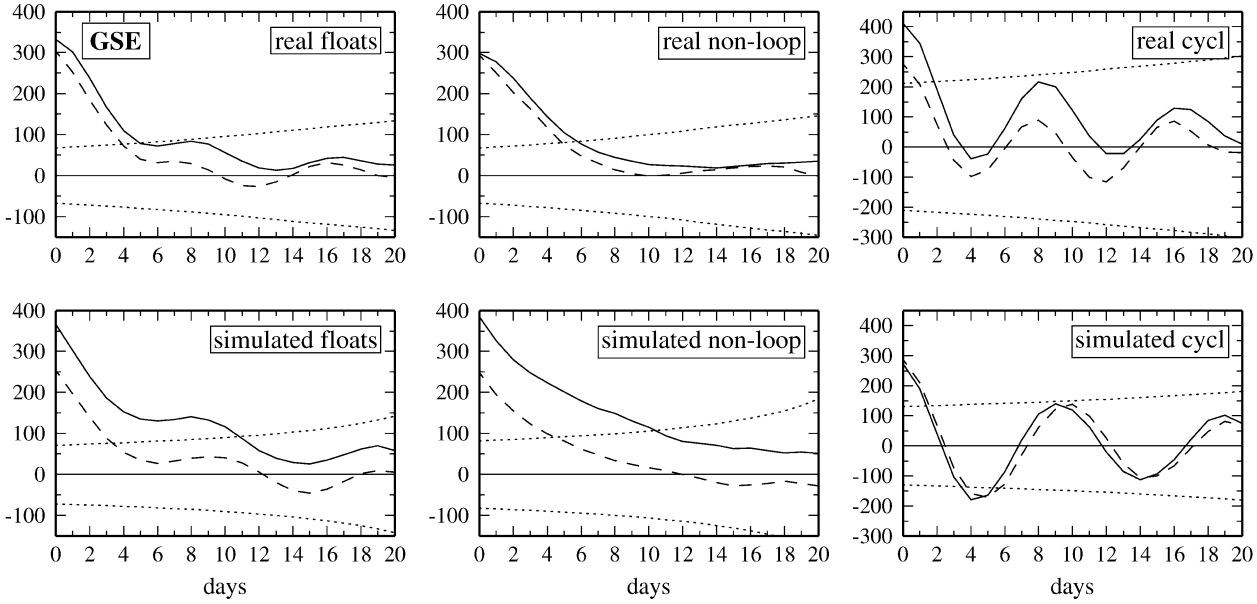

FIG. 12. Velocity autocovariance functions obtained in the Gulf Stream extension region GSE.

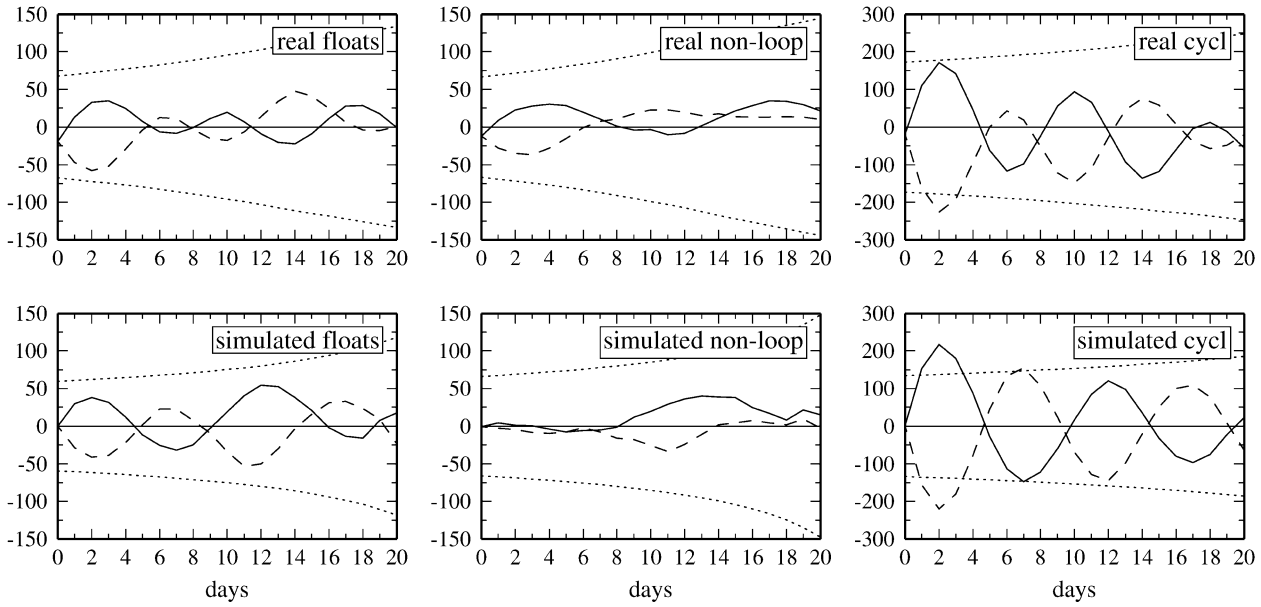

FIG. 13. Same as in Fig. 12, but for the velocity cross-covariance functions.

The V_{rms} values associated with the nonlooping trajectories are higher than or on the same order of magnitude as the looper velocities, as anticipated by the autocovariance function results. The oscillation time scale T_w is rather noisy in GSW, while it ranges between 13 and 16 days in GSE.

We simulated only two groups of floats in these regions, the nonloopers and the cyclonic trajectories, because the anticyclonic data were too few to modify significantly the overall results. The autocovariance and cross-covariance functions computed from the synthetic trajectories are displayed in the three lower panels of Figs. 10 and 11 for region GSW, and in the lower panels of Figs. 12 and 13 for GSE. When comparing the outcome with the corresponding statistics from the real data in region GSW, we notice that the simulations are not very successful at reproducing the overall autocovariances and cross covariances, although the errors are large for any definitive conclusion to be drawn. This suggests that in areas dominated by highly coherent jets rather than vortices and eddies, different parameterization schemes should be employed. The applicability of a nonlinear two-dimensional LS model to wave structure dominated dynamics is investigated for example by Reynolds (2002b).

The simulations performed in region GSE, however, provide statistics very comparable to those computed from the real Lagrangian data, suggesting that the bimodal spin distributed model applies properly in this area.

3) REGION AZ

This area (Fig. 2b) is located north of the Azores Current (Ollitrault and Colin de Verdiere 2002b) and is characterized by a weak eastward mean flow to the north and by an eastward circulation (Azores Current signal) to the south. The regional average flow has a zonal component of -1.1 ± 0.5 cm s^{-1} and an even weaker meridional mean velocity equal to 0.8 ± 0.5 cm s^{-1}. The area is the most quiescent of all the northwestern Atlantic regions considered in this paper, with an overall eddy kinetic energy approximately equal to 68 ± 4 cm^2 s^{-2} and an rms velocity ≈ 11.7 cm s^{-1}. Therefore, the eddy field is stronger than the mean flow also for this case.

Most of the Lagrangian data in AZ are 700-m floats released during the TOPOGULF and the Newfoundland Basin Experiment (Schmitz 1985). Since many looping floats were launched spatially close to each other and within short time scales, we performed a subsampling procedure by considering only those trajectories that were initially farther than 100 km apart. About 74% of the trajectories remain in the region for less than 40 days, while 14% of them stay for periods between 3 and 9 months mainly because they are trapped inside nearly steady coherent vortices. The region has the highest percentage of loopers (40%, see Table 2), mostly cyclonic and possibly due to rotating structures originating through instabilities of the subtropical front (Pingree and Sinha 2001). The number of independent data, n^*, is equal to 296.

The autocovariance and cross-covariance functions computed from the whole Lagrangian dataset in this region and from the separated subsets of the nonloopers and cyclonic loopers are displayed in the upper three panels of Figs. 14 and 15, respectively. The overall velocity autocovariance shows a weak subdiffusive behavior, while the corresponding cross-covariance func-

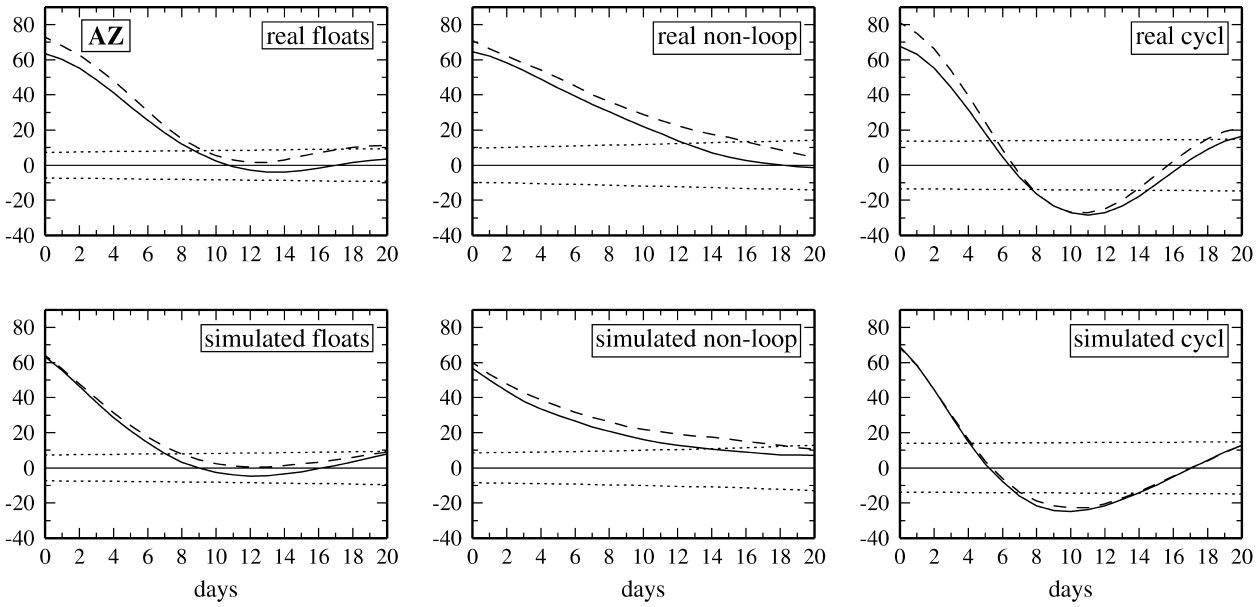

FIG. 14. Velocity autocovariance functions computed in the Azores Current region AZ.

tion is approximately sinusoidal with oscillation time scale ≈20 days. This pattern appears to be induced by the dominant cyclonic trajectories (whose statistics are shown in the upper-right panels of Figs. 14 and 15), since the nonlooping floats give rise to exponentially decaying autocovariances and statistically nonsignificant cross covariances (upper-middle panels in Figs. 14 and 15). An important difference between AZ and the previously analyzed regions is that the loopers are as energetic as the nonloopers, suggesting that their formation mechanism is associated with more quiescent dynamical regimes.

We applied the first-order model with the bimodal spin distribution also in this region. The results in terms of model parameters (Table 3) are characterized by longer decorrelation and oscillation time scales than those obtained for the other North Atlantic areas. The cyclonic loopers, for example, have T_L ranging between 8 and 11 days, and $T_w \approx 30$ days. The nonlooping floats exhibit even longer Lagrangian decorrelation scales on the order of 14 days.

The results from the numerical integration of Eq. (2) give rise to autocovariance and cross-covariance functions that are shown in the lower three panels of Figs. 14 and 15. We notice that the simulated trajectories are able to reproduce the statistics obtained from the real data, proving that, also for region AZ, the bimodality hypothesis is sufficient to describe the main features of the eddy field.

5. Parameter distribution and bimodality

The statistical results of section 4 have shown that the approach of applying a first-order Lagrangian stochastic model with a bimodal distribution of the spin parameter is successful in describing the main features of the mesoscale eddy field. Some quantitative differences persist, however, between the modeled statistics and the results obtained from the real data. This raises the question of how appropriate the bimodal distribution is in quantitative terms, and whether other more complex distributions could improve the results. In an attempt to address this question, we have estimated the parameter Ω and the eddy kinetic energy for each trajectory (longer than 20 days) using the method described in appendix B.

We have then considered their resulting distribution, by plotting Ω versus EKE for each northwestern Atlantic region (Fig. 16). The various colors in the plot denote different ranges of trajectory length: black for floats shorter than 50 days, blue for floats ranging between 50 and 100 days, and red for trajectories longer than 100 days. Only the Ω error bars are displayed for the sake of clarity, but the EKE errors are generally smaller. The error over the angular velocity does not depend only on the number of float days, but also on the sampling interval Δt (see appendix B). We identify the loopers as the trajectories with Ω significantly different from 0 ($|\Omega| \geq 0.1$ days^{-1}, corresponding to an oscillation time scale $T_w \leq 60$ days). Notice that this definition is not exactly equivalent to the Richardson (1993) criterion. There are in fact a few trajectories (18% of the total loopers) that have significant Ω without looping twice in the same direction, especially in correspondence of the meanders in the Gulf Stream regions. However, as mentioned in section 4, the statistical results are robust and independent from the specific looper definition used.

The results in Fig. 16 show an interesting scenario that can be outlined as follows.

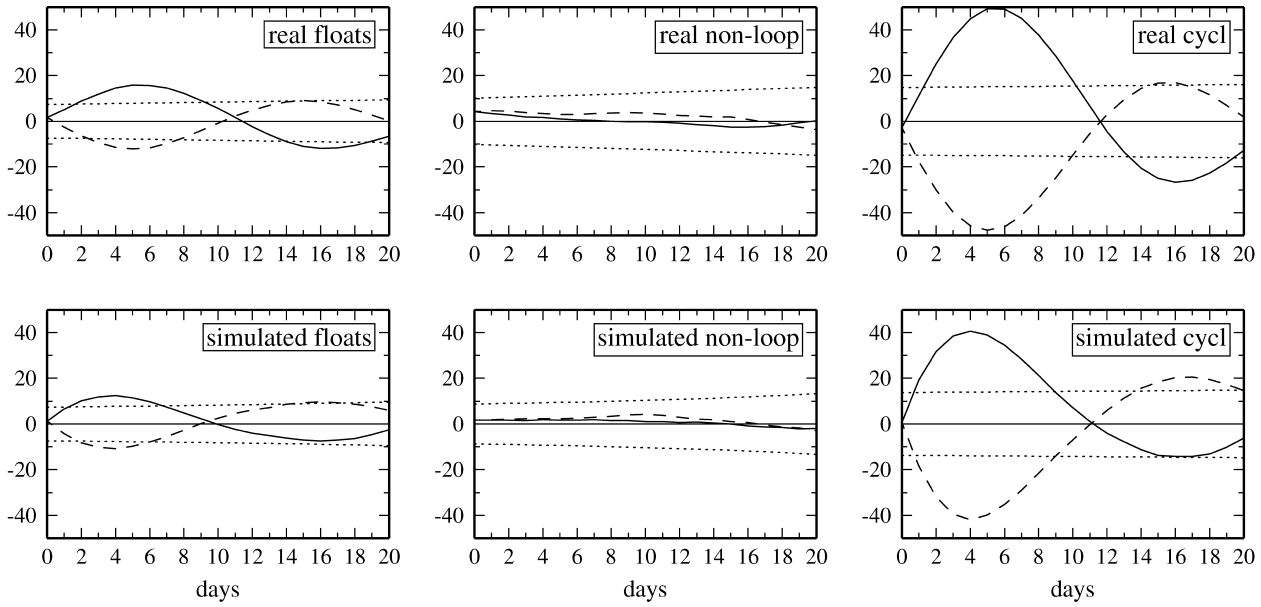

FIG. 15. Same as in Fig. 14, but for the velocity cross-covariance functions.

1) In the recirculation regions RECW and RECE, and in region AZ (top two panels and lower panel in Fig. 16, respectively), there are clearly a number of floats characterized by nonsignificant Ω and weak EKE (in the range of 80–100 cm^2 s^{-2}, with typical $V_{\rm rms} \leq 10$ cm s^{-1}). They represent what we have called the family of nonloopers.

   In RECW and RECE distinctive loopers are also identifiable, with high values of both Ω ($\approx$0.5 days^{-1} in amplitude) and EKE (higher than 600 cm^2 s^{-2}, $V_{\rm rms} \approx 35$ cm s^{-1}). They are representative of cold-core Gulf Stream rings (cyclonic floats) and energetic lenses (anticyclonic floats). Although these looping features are not numerous, they dominate the statistics of the loopers because they are energetic and able to trap the floats for long periods of time.

   Other trajectories in the recirculation regions are characterized by intermediate values of both Ω ($\approx$0.2–0.4 days^{-1} in amplitude) and EKE (ranging between 100 and 300 cm^2 s^{-2}, with typical $V_{\rm rms} \approx$ 20 cm s^{-1}). These loopers are less distinctive and shorter in time, although they are most probably responsible for the complex behavior of the looping float statistics in region RECE (section 4b).
2) In the Azores Current region AZ, there are also a number of looping trajectories, but they exhibit low values of Ω ($\approx$0.2 days^{-1}) and EKE (60–80 cm^2 s^{-2}).
3) In the Gulf Stream extension regions (two middle panels in Fig. 16), the scenario is more complex, probably because of the influence of fluctuating meanders and wave structures. In GSE, it is easier to identify a family of nonloopers (characterized by higher EKE levels than those typical of the non-looping floats in the other regions) and a group of loopers exhibiting scattered values of Ω ($\approx$0.2–0.6 days^{-1}).

The scattering of Ω and EKE for the loopers, observed in the various regions, could be due to the coexistence of vortices with differing dynamics and/or to the different type of sampling within vortices of the same kind. Hydrographic surveys of Gulf Stream rings, in fact, have revealed that mainly cold-core, but also warm-core rings are characterized by an inner core rotating approximately as a solid body (Olson 1980; Joyce 1984). This means that the azimuthal velocity increases linearly with the distance from the ring center, and the angular velocity remains constant within the vortex core. Outside the core, however, the azimuthal velocity falls exponentially away from the ring center, and a similar behavior is expected for Ω. Therefore, if the float is moving on the edge of a vortex, its angular velocity and EKE are lower than what they would be in case the float were sampling the eddy core.

To distinguish between sampling effects and the actual influence of different vortices is not an easy task with the available data. We have compared $V_{\rm rms}$, r, and Ω estimated from the loopers characterized by intermediate EKE levels with the same parameters obtained from the highly energetic looping floats, and we have also looked closely at their looping trajectories. The conclusion is that both possibilities are likely to occur. Some of the loopers with intermediate values of EKE/Ω provide significantly higher average radii than those estimated by the high-EKE loopers, suggesting that they are moving on the edge of vortices rather than inside the eddy cores. In contrast, other looping trajectories do

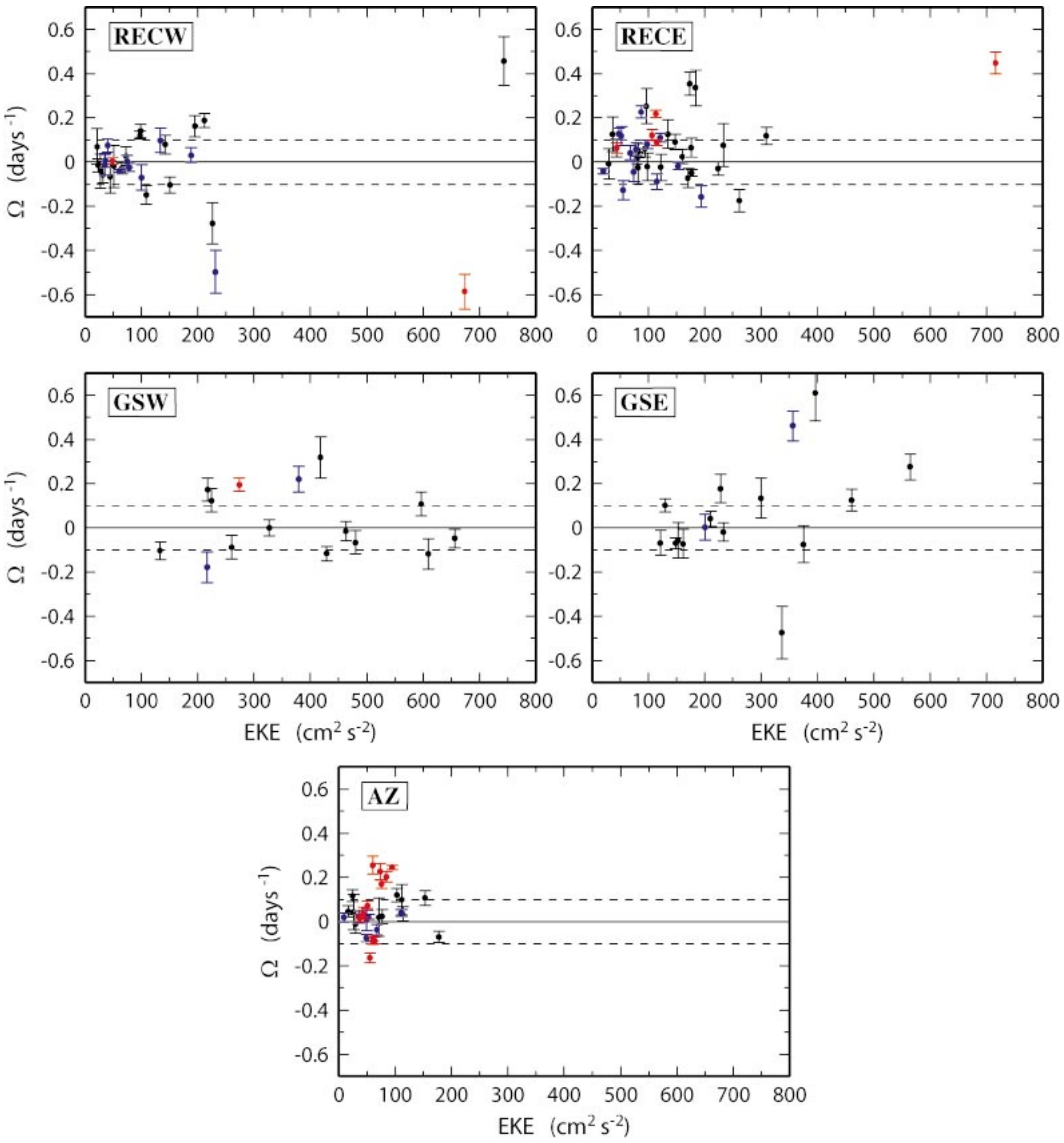

FIG. 16. Plot of Ω vs the eddy kinetic energy computed from single trajectories in the five subregions of the northwestern Atlantic. The angular velocity error bars are also drawn. Various colors have been used to denote the actual length of the trajectories: black for floats shorter than 50 days, blue for floats ranging between 50 and 100 days, and red for trajectories longer than 100 days.

seem to represent different types of eddy structures, since they exhibit non–significantly different average radii and a proportionality relationship between V_{rms} and Ω.

In summary, these results indicate that, although the simplifying assumption of bimodality is able to capture the main statistical characteristics of the data, the actual parameter distribution is probably more complex. From the theoretical and numerical point of view, there is no problem in using different types of distributions (Berloff and McWilliams 2003; Reynolds 2002b, 2003b). For example, the results shown in Fig. 16 could be used directly to simulate trajectories and reproduce the details of the statistics in section 4. We believe, however, that this would not really contribute to our understanding of the phenomenon because the distribution from the present data is too incomplete and too strongly influenced by the specific sampling to be considered general.

Another point that was not addressed in the present work because of lack of data is the application of an LS model that takes into account the possible transition of floats between looping and nonlooping regimes. Such a model would be more representative of the real oceanic processes over time scales comparable to, or greater than, the transition time scale. However, we feel that the present data coverage is not sufficient to provide reliable statistics of number of particles that enter/exit the looping structures. Further investigations will be

necessary to identify the actual parameter distribution in some detail, and the float transition between looping and nonlooping events. A useful tool will be the use of synthetic Lagrangian data simulated by high-resolution ocean models, so that sampling limitation will not be a problem, and Eulerian velocity fields will also be available (Garraffo et al. 2001a,b).

6. Summary and concluding remarks

In this paper, an analysis of mesoscale Lagrangian turbulence in the subsurface North Atlantic is presented. The basic strategy, commonly used in oceanography, consists in first identifying geographical regions that are approximately homogeneous in terms of both dynamical and statistical properties (EKE distribution). The mean flow **U** is then computed in these regions and subtracted from the total velocity. The residual velocity **u** is considered as representative of mesoscale eddy field and analyzed as homogeneous turbulence. The outstanding question behind this approach is of course whether the hypothesis of scale separation between **U** and **u** and the hypothesis of **u** homogeneity actually hold true in the considered regions (Landau and Lifshitz 1981). Of the five subregions identified in this paper, the most western jet extension area (GSW) is probably the most critical in terms of scale separation, since the variability is significantly influenced by the meandering jet. In fact, the results of the analysis seem to be less clear and reliable in this specific region. In all of the other areas, on the other hand, the decomposition appears solid, with a weak mean flow and a mesoscale turbulent field with very well defined properties.

Our main result is that mesoscale turbulence can be viewed in each region as the superposition of two different regimes, corresponding to looping and nonlooping trajectories, and that both can be parameterized using a simple first-order LS model with spin Ω. The spin is considered as a random parameter (Reynolds 2002a; Berloff and McWilliams 2003) and approximately as a bimodal process, reflecting the distribution of loopers (finite Ω) and nonloopers (zero Ω). The loopers can be further separated in cyclonic and anticyclonic trajectories, but only one family is found to be dominant in each region. The first-order Lagrangian stochastic model is found to be very effective in reproducing the main statistical properties observed from the data.

Physically, the nonlooping trajectories characterize the background flow field, and they tend to disperse diffusively as in random turbulence. They correspond to the majority of the floats ($\approx$85%–60% of the data, depending on the region), but they are generally less energetic and shorter. The loopers characterize the coherent vortices and, although less numerous, they tend to dominate the statistics because they are generally more energetic and tend to trap particles for a long time, exhibiting a subdiffusive behavior. The superposition of loopers and nonloopers can produce superdiffusive statistics for the overall dataset.

At the conceptual level, the resulting scenario is strongly reminiscent of two-dimensional turbulence (Elhmaidi et al. 1993; Provenzale et al. 1995; Provenzale 1999). The statistics appear highly influenced by coherent structures, which are likely to be also responsible for the observed non-Gaussianity in the velocity field (Bracco et al. 2000). At a more detailed level, however, there might be significant departures from two-dimensional turbulence dynamics. In particular, the nature of coherent vortices may be different. Vortex characteristics as shown by the data are highly local and change significantly in the various regions, probably because of the action of different forcings. Energetic lenses (anticyclonic) and Gulf Stream rings (cyclonic) are found in the recirculation regions, while much less energetic vortices characterize the Azores Current area. Depending on the vortex characteristics, the properties of particle trapping and mass exchanges might also be significantly different from those found in two-dimensional turbulence (Elhmaidi et al. 1993).

The present results open a new avenue for the interpretation and parameterization of Lagrangian mesoscale turbulence in the ocean in presence of coherent structures. The identification of a suitable LS model in regions characterized by complex eddy dynamics is, in fact, an important step forward in local parameterizations of turbulent transport. Future investigations can be foreseen, aimed at refining the appropriate models and improving their quantitative performance. The bimodal assumption for the LS model parameter distribution, for instance, is certainly oversimplified, as suggested by the plot of Ω against EKE computed from the single trajectories. The present data coverage, however, is not sufficient to provide more detailed information on the actual distribution structure and on the probability of a float to transit between looping and nonlooping flow regimes. Further investigations using synthetic Lagrangian data in high-resolution models might help in addressing these points.

Also, an important point to be assessed in the future is whether the relevance of coherent structures is specific to highly energetic, strongly sheared regions such as the ones considered here, or whether it is a more pervasive feature of subsurface flows. Below the ocean surface, in fact, coherent structures might survive longer than at the surface, because of the absence of direct randomizing forcing such as synoptic winds. Further subsurface data and turbulent statistical analyses are needed to answer this question.

The present analysis provides indications for transport parameterizations in coarse-grain GCMs. Lagrangian stochastic models are often used in conjunction with OGCM velocity outputs to simulate transport of pollutants or of biological quantities that can be considered approximately as passive tracers (Cowen et al. 2000, 2003). Very simple first-order, one-dimensional LSMs

with constant parameters are often used (e.g., Dutkiewicz et al. 1993; Falco et al. 2000). The present results indicate that the use of two-dimensional models with distributed spin is more appropriate in presence of coherent structures and it provides information on parameter distribution in the subsurface North Atlantic. When considering global (i.e., basinwide) applications, the effect of inhomogeneities will have to be introduced by means of modified LSMs, whose drift terms take into account the spatial distribution of the parameters (e.g., Berloff and McWilliams 2002). The approach is expected to provide useful results in regions where the scale separation holds true and where the local homogeneity allows one to correctly identify the LSM parameters, as in most of the subregions considered here. Applicability to highly inhomogeneous and nonlinear areas, such as the jet and its extension, are potentially more problematic.

Acknowledgments. The authors thank sincerely Leonid Piterbarg for important suggestions on statistics and error estimations, and Bill Johns, Don Olson, Enrico Zambianchi, Zulema Garraffo, Eric Chassignet, and Claudia Pasquero for many stimulating discussions. Authors M. Veneziani and A. Griffa were supported by the National Science Foundation Grant OCE-9811358, the Office of Naval Research Grant N00014-97-1-0620, and the Italian National Research Council (CNR) through the SINAPSI Project. Author A. M. Reynolds was partially supported by the BBSRC through a core strategic grant. Author A. J. Mariano was supported through ONR Grant N00014-99-1-0049.

APPENDIX A

Estimate of the Mean Flow by Bicubic Spline Interpolation

The results of the bicubic spline interpolation depend on four parameters, the knot spacing, which is related to the number of finite elements of the interpolation function, and three weights, which are associated with uncertainties in the data and in the first and second derivatives of the interpolated field (Inoue 1986). The data weight depends on our confidence of the Lagrangian velocity data and can be chosen proportional to the inverse of the estimated variance of the eddy field. The tension is associated with the first derivative of the splined flow, and its value has to minimize fluctuations at the boundaries. It is typically fixed at 0.99 (Mariano and Brown 1992). The roughness is related to the second derivative—that is, to the ''curvature'' of the interpolated field—and controls the wavenumber content of the results. Bauer et al. (1998) showed that, at fixed knot spacing, data weight, and tension, the roughness ρ can be optimized in such a way to minimize the energy in the fluctuation field at low frequency.

We have performed a sensitivity analysis by varying the spline parameters and testing the robustness of the eddy statistics. The knot spacing has been varied between 1° and 3°, while two values for the data weight have been chosen, corresponding to different binned eddy kinetic energies. The roughness has been considered in the range 10^{-2}–1000, changing its value by one order of magnitude at a time.

It has been found that, for all the knot spacing and data weight choices, the eddy statistics tend to behave asymptotically at high values of ρ, with the autocovariance and cross-covariance structures becoming independent from the specific value of roughness. This suggests that the eddy statistics are robust, independent from the particular estimate of the interpolated mean flow.

APPENDIX B

Estimate of the Model Parameters

The parameters of the two-dimensional, first-order Lagrangian stochastic model described by Eq. (2) are the velocity variance σ^2, the decorrelation time scale T_L, and the angular velocity Ω. They can be estimated as follows.

The velocity variance is given by the autocovariance function at 0 time lag, while T_L is evaluated by making the a priori assumption that a two-dimensional first-order model applies. The decorrelation scale is then estimated by using the theoretical autocorrelation function given in Eq. (4). We obtain the formula

$$T_L = 2\tau\left\{\ln\left[\frac{R(0)^2}{2R(\tau)^2 - R(0)R(2\tau)}\right]\right\}^{-1}, \qquad \text{(B1)}$$

where R is either the zonal or the meridional autocorrelation function according to what component of the decorrelation scale we are computing. Because of large errors of the autocorrelation estimate, we calculated different values of T_L by choosing $\tau = \Delta t, 2\Delta t, 3\Delta t, \ldots$, until we obtained a saturation level for the decorrelation scale.

The angular velocity Ω is evaluated through Eq. (3), where the mean spin $\langle ds \rangle$ is estimated as

$$\begin{aligned}\langle ds \rangle &\equiv \langle u dv - v du \rangle \sim \langle u(t)[v(t + \Delta t) - v(t)] \\ &\quad - v(t)[u(t + \Delta t) - u(t)]\rangle \\ &= \langle u(t)v(t + \Delta t) - v(t)u(t + \Delta t)\rangle \\ &= R_{uv}(\Delta t) - R_{vu}(\Delta t). \qquad \text{(B2)}\end{aligned}$$

The accuracy of this estimate depends not only on the total number of observations, but also on the sampling period Δt. In fact, Δt must be much shorter than Ω^{-1} in order for the oscillations in the data statistics to be resolved.

The oscillation time scale T_w is simply given by $2\pi\Omega^{-1}$, while the average vortex radius r is estimated as $V_{\text{rms}}\Omega^{-1}$.

Error estimation of these parameters is not straight-

forward. We adopted the ''bootstrap'' technique, through which a series of numerical experiments is carried out to simulate the independent realizations necessary for the error evaluation. Specifically in our case, we simulated a certain number of float trajectories so as to reproduce the number of observations characteristic of either the looper or the nonlooper dataset. The simulation is repeated as many times as the number of independent realizations we wish to reproduce (typically 10). A lower bound for the parameter error is computed as standard deviation of the estimates carried out in each realization.

REFERENCES

Bauer, S., M. S. Swenson, A. Griffa, A. J. Mariano, and K. Owens, 1998: Eddy-mean flow decomposition and eddy-diffusivity estimates in the tropical Pacific Ocean. 1. Methodology. *J. Geophys. Res.,* **103,** 30 855–30 871.

——, ——, and ——, 2002: Eddy-mean flow decomposition and eddy-diffusivity estimates in the tropical Pacific Ocean. 2. Results. *J. Geophys. Res.,* **107,** 3154, doi:10.1029/2001JC000613.

Berloff, P. S., and J. C. McWilliams, 2002: Material transport in oceanic gyres. Part II: Hierarchy of stochastic models. *J. Phys. Oceanogr.,* **32,** 797–830.

——, and ——, 2003: Material transport in oceanic gyres. Part III: Randomized stochastic models. *J. Phys. Oceanogr.,* **33,** 1416–1445.

——, ——, and A. Bracco, 2002: Material transport in oceanic gyres. Part I: Phenomenology. *J. Phys. Oceanogr.,* **32,** 764–796.

Borgas, M. S., T. K. Flesch, and B. L. Sawford, 1997: Turbulent dispersion with broken reflectional symmetry. *J. Fluid Mech.,* **279,** 69–99.

Bower, A. S., and Coauthors, 2002: Directly measured mid-depth circulation in the northeastern North Atlantic Ocean. *Nature,* **419,** 603–607.

Bracco, A., J. H. LaCasce, and A. Provenzale, 2000: Velocity probability density functions for oceanic floats. *J. Phys. Oceanogr.,* **30,** 461–474.

——, E. P. Chassignet, Z. D. Garraffo, and A. Provenzale, 2003: Lagrangian velocity distributions in a high-resolution numerical simulation of the North Atlantic. *J. Atmos. Oceanic Technol.,* **20,** 1212–1220.

Brown, O. B., P. C. Cornillon, S. R. Emmerson, and H. M. Carle, 1986: Warm core rings: A statistical study of their behavior. *Deep-Sea Res.,* **33,** 1459–1473.

Brundage, W. L., and J. P. Dugan, 1986: Observations of an anticyclonic eddy of 18°C water in the Sargasso Sea. *J. Phys. Oceanogr.,* **16,** 717–727.

Cheney, R. E., W. H. Gemmill, M. K. Shank, P. L. Richardson, and D. C. Webb, 1976: Tracking a Gulf Stream ring with SOFAR floats. *J. Phys. Oceanogr.,* **6,** 741–749.

Cowen, R. K., K. M. M. Lwiza, S. Sponaugle, C. B. Paris, and D. B. Olson, 2000: Connectivity of marine populations: Open or closed? *Science,* **287,** 857–859.

——, C. B. Paris, D. B. Olson, and J. L. Fortuna, 2003: The role of long distance dispersal versus local retention in replenishing marine populations. *Gulf Caribb. Res.,* **14** (2), 129–137.

Davis, R. E., 1991: Observing the general circulation with floats. *Deep-Sea Res.,* **38** (Suppl.), 531–571.

——, 1998: Preliminary results from directly measuring mid-depth circulation in the tropical and South Pacific. *J. Geophys. Res.,* **103,** 24 619–24 639.

Dutkiewicz, S., A. Griffa, and D. B. Olson, 1993: Particle diffusion in a meandering jet. *J. Geophys. Res.,* **98,** 16 487–16 500.

Elhmaidi, D., A. Provenzale, and A. Babiano, 1993: Elementary topology of two-dimensional turbulence from a Lagrangian viewpoint and single particle dispersion. *J. Fluid Mech.,* **257,** 533–558.

Falco, P., A. Griffa, P.-M. Poulain, and E. Zambianchi, 2000: Transport properties in the Adriatic Sea as deduced from drifter data. *J. Phys. Oceanogr.,* **30,** 2055–2071.

Figueroa, H. A., and D. B. Olson, 1989: Lagrangian statistics in the South Atlantic as derived from SOS and FGGE drifters. *J. Mar. Res.,* **47,** 525–546.

Fratantoni, D. M., 2001: North Atlantic surface circulation during the 1990's observed with satellite-tracked drifters. *J. Geophys. Res.,* **106,** 22 067–22 093.

Freeland, H., P. Rhines, and H. T. Rossby, 1975: Statistical observations of the trajectories of neutrally buoyant floats in the North Atlantic. *J. Mar. Res.,* **33,** 383–404.

Garraffo, Z. D., A. Griffa, A. J. Mariano, and E. P. Chassignet, 2001a: Lagrangian data in a high resolution numerical simulation of the North Atlantic. II: On the pseudo-Eulerian averaging of Lagrangian data. *J. Mar. Syst.,* **29,** 177–200.

——, A. J. Mariano, A. Griffa, C. Veneziani, and E. P. Chassignet, 2001b: Lagrangian data in a high resolution numerical simulation of the North Atlantic. I: Comparison with in-situ drifter data. *J. Mar. Syst.,* **29,** 157–176.

Griffa, A., 1996: Applications of stochastic particle models to oceanographic problems. *Stochastic Modeling in Physical Oceanography,* R. Adler, P. Muller, and B. Rozovskii, Eds., Birkhäuser Verlag, 114–140.

Inoue, H., 1986: A least-squares smooth fitting for irregularly spaced data: Finite-element approach using the cubic B-spline basis. *Geophysics,* **51,** 2051–2066.

Joyce, T. M., 1984: Velocity and hydrographic structure of a Gulf Stream warm-core ring. *J. Phys. Oceanogr.,* **14,** 936–947.

Klein, H., and E. Mittelstaedt, 1992: Currents and dispersion in the abyssal Northeast Atlantic. Results from the NOAMP Field Program. *Deep-Sea Res.,* **39,** 1727–1745.

Krauss, W., and C. W. Boning, 1987: Lagrangian properties of the eddy fields in the northern Atlantic as deduced from satellite-tracked buoys. *J. Mar. Res.,* **45,** 259–291.

LaCasce, J. H., 2000: Floats and *f/H. J. Mar. Res.,* **58,** 61–95.

Landau, L. D., and E. M. Lifshitz, 1981: *Physical Kinetics.*Vol. 10. Butterworth-Heinemann, 625 pp.

Lavender, K. L., R. E. Davis, and W. B. Owens, 2000: Mid-depth recirculation observed in the interior Labrador and Irminger Seas by direct velocity measurements. *Nature,* **407,** 66–69.

Leaman, K. D., and P. S. Vertes, 1996: Topographic influences on recirculation in the deep western boundary current: Results from RAFOS float trajectories between the Blake–Bahama Outer Ridge and the San Salvador ''Gate.'' *J. Phys. Oceanogr.,* **26,** 941–961.

Mariano, A. J., and O. B. Brown, 1992: Efficient objective analysis of heterogeneous and nonstationary fields via the parameter matrix. *Deep-Sea Res.,* **39,** 1255–1271.

Ollitrault, M., and A. Colin de Verdiere, 2002a: SOFAR floats reveal midlatitude intermediate North Atlantic general circulation. Part I: A Lagrangian descriptive view. *J. Phys. Oceanogr.,* **32,** 2020–2033.

——, and ——, 2002b: SOFAR floats reveal midlatitude intermediate North Atlantic general circulation. Part II: An Eulerian statistical view. *J. Phys. Oceanogr.,* **32,** 2034–2053.

Olson, D. B., 1980: The physical oceanography of two rings observed by the Cyclonic Ring Experiment. Part II: Dynamics. *J. Phys. Oceanogr.,* **10,** 514–528.

Owens, W. B., 1984: A synoptic and statistical description of the Gulf Stream and subtropical gyre using SOFAR floats. *J. Phys. Oceanogr.,* **14,** 104–113.

——, 1991: A statistical description of the mean circulation and eddy variability in the northwestern Atlantic using SOFAR floats. *Progress in Oceanography,* Vol. 28, Pergamon Press, 257–303.

Pasquero, C., A. Provenzale, and A. Babiano, 2001: Parameterization of dispersion in two-dimensional turbulence. *J. Fluid Mech.,* **439,** 279–303.

Patterson, S. L., 1985: Surface circulation and kinetic energy distributions in the Southern Hemisphere oceans from FGGE drifting buoys. *J. Phys. Oceanogr.,* **15,** 865–884.

Pingree, R., and B. Sinha, 2001: Westward moving waves or eddies (storms) on the Subtropical/Azores front near 32.5°N? Interpretation of the Eulerian currents and temperature records at moorings 155 (35.5° W) and 156 (34.4° W). *J. Mar. Syst.,* **29,** 239–276.

Poulain, P.-M., 2001: Adriatic Sea surface circulation as derived from drifter data between 1990 and 1999. *J. Mar. Syst.,* **29,** 3–32.

——, and P. P. Niiler, 1989: Statistical analysis of the surface circulation in the California Current System using satellite-tracked drifters. *J. Phys. Oceanogr.,* **19,** 1588–1603.

Price, J. F., T. M. McKee, W. B. Owens, and J. R. Valdes, 1987: Site L SOFAR float experiment, 1982–85. Woods Hole Oceanographic Institution Tech. Rep. WHOI-97-52, 289 pp. [Available online at http://www.ntis.gov.]

Priestley, M. B., 1981: *Spectral Analysis and Time Series.* Academic Press, 890 pp.

Provenzale, A., 1999: Transport by coherent barotropic vortices. *Annu. Rev. Fluid Mech.,* **31,** 55–93.

——, A. Babiano, and B. Villone, 1995: Single-particle trajectories in two-dimensional turbulence. *Chaos, Solitons Fractals,* **5,** 2055–2071.

Rees, J. M., and E. M. Gmitrowicz, 1989: Dispersion measurements from SOFAR floats on the Iberian abyssal plain. *Interim Oceanographic Description of the North-East Atlantic Site for the Disposal of Low-Level Radioactive Waste,* Vol. 3, F. Nyffeler and W. Simmons, Eds., Nuclear Energy Agency, OECD, 64–67.

Reynolds, A. M., 2002a: On Lagrangian stochastic modelling of material transport in oceanic gyres. *Physica D,* **172,** 124–138.

——, 2002b: Lagrangian stochastic modeling of anomalous diffusion in two-dimensional turbulence. *Phys. Fluids,* **14,** 1442–1449.

——, 2003a: Third-order Lagrangian stochastic modeling. *Phys. Fluids,* **15,** 2773–2777.

——, 2003b: On the application of nonextensive statistics to Lagrangian turbulence. *Phys. Fluids,* **15,** L1–L4.

Richardson, P. L., 1980: Anticyclonic eddies generated near the Corner Rise seamounts. *J. Mar. Res.,* **38,** 673–686.

——, 1993: A census of eddies observed in North Atlantic SOFAR float data. *Progress in Oceanography,* Vol. 31, Pergamon Press, 1–50.

Riser, S. C., 1982: The quasi-Lagrangian nature of SOFAR floats. *Deep-Sea Res.,* **29,** 1587–1602.

——, and H. T. Rossby, 1983: Quasi-Lagrangian structure and variability of the subtropical western North Atlantic circulation. *J. Mar. Res.,* **41,** 127–162.

Risken, H., 1989: *The Fokker–Planck Equation: Methods of Solution and Applications.* Springer-Verlag, 472 pp.

Rossby, H. T., A. D. Voorhis, and D. Webb, 1975: A quasi-Lagrangian study of mid-ocean variability using long-range SOFAR floats. *J. Mar. Res.,* **33,** 355–382.

——, J. F. Price, and D. Webb, 1986: The spatial and temporal evolution of a cluster of SOFAR floats in the POLYMODE Local Dynamics Experiment (LDE). *J. Phys. Oceanogr.,* **16,** 428–442.

Rupolo, V., V. Artale, B. L. Hua, and A. Provenzale, 1996: Lagrangian velocity spectra at 700 m in the western North Atlantic. *J. Phys. Oceanogr.,* **26,** 1591–1607.

Sawford, B. L., 1991: Reynolds number effects in Lagrangian stochastic models of turbulent dispersion. *Phys. Fluids,* **A3,** 1577–1586.

——, 1999: Rotation of trajectories in Lagrangian stochastic models of turbulent dispersion. *Bound.-Layer Meteor.,* **93,** 411–424.

Schmitz, W. J., Jr, 1985: SOFAR float trajectories associated with the Newfoundland Basin. *J. Mar. Res.,* **43,** 761–778.

——, J. F. Price, P. L. Richardson, W. B. Owens, D. C. Webb, R. E. Cheney, and H. T. Rossby, 1981: A preliminary exploration of the Gulf Stream system with SOFAR floats. *J. Phys. Oceanogr.,* **11,** 1194–1204.

Sciremammano, F., Jr., 1979: A suggestion for the presentation of correlations and their significance levels. *J. Phys. Oceanogr.,* **9,** 1273–1276.

Spall, M. A., P. L. Richardson, and J. F. Price, 1993: Advection and eddy mixing in the Mediterranean salt tongue. *J. Mar. Res.,* **51,** 797–818.

Sundermeyer, M. A., and J. F. Price, 1998: Lateral mixing and the North Atlantic Tracer Release Experiment: Observations and numerical simulations of Lagrangian particles and passive tracer. *J. Geophys. Res.,* **103,** 21 481–21 497.

Swenson, M. S., and P. P. Niiler, 1996: Statistical analysis of the surface circulation of the California Current. *J. Geophys. Res.,* **101,** 22 631–22 645.

Taylor, G. I., 1921: Diffusion by continuous movements. *Proc. London Math. Soc.,* **20,** 196–212.

Tennekes, H., and J. L. Lumley, 1972: *A First Course in Turbulence.* MIT Press, 300 pp.

Thomson, D. J., 1987: Criteria for the selection of stochastic models of particle trajectories in turbulent flows. *J. Fluid Mech.,* **180,** 529–556.

Zenk, W., K. S. Tokos, and O. Boebel, 1992: New observations of meddy movement south of the Tejo Plateau. *Geophys. Res. Lett.,* **19,** 2389–2392.

Zhang, H.-M., M. D. Prater, and T. Rossby, 2001: Isopycnal Lagrangian statistics from the North Atlantic Current RAFOS floats observations. *J. Geophys. Res.,* **106,** 13 817–13 836.